

Dynamics of Multi-Strain Epidemic Models and the Impact of
Masking and Vaccination

by

Ravindu Gimantha Upasena

Bachelor of Engineering (Honours) in Mechatronics Engineering, Monash
University Malaysia, 2019

A Thesis Submitted in Partial Fulfilment of
the Requirements for the Degree of

Master of Science

In the Graduate Academic Unit of Mathematics and Statistics

Supervisor: Lin Wang, Ph.D, Mathematics and Statistics

Examining Board: James Watmough, Ph.D, Mathematics and Statistics
Zhen Lei, Ph.D., Civil Engineering

This thesis is accepted by the
Dean of Graduate Studies

THE UNIVERSITY OF NEW BRUNSWICK

April, 2025

© Ravindu Gimantha Upasena, 2025

Abstract

Mathematical modelling plays a pivotal role in informing public health strategies for infectious disease control. Although numerous studies have investigated multi-strain epidemic dynamics, key aspects such as asymptomatic transmission and waning immunity are often excluded. This thesis develops and analyzes two compartmental models to address these limitations.

The first model, an SIARS framework, examines multi-strain transmission in a homogeneous population without interventions. Strain-specific basic reproduction numbers are derived, and analytical conditions for the existence and stability of equilibria are established. Numerical simulations further illustrate the analytical results.

The second model, an SVIARS framework, incorporates mask usage and vaccination in a non-homogeneous population. Despite the model's high dimensionality, strain-specific reproduction numbers are identified, enabling an explicit expression for the overall basic reproduction number. Numerical analyses quantify the impact of intervention parameters and determine critical efficacy thresholds.

The results offer practical insights for mitigating multi-strain outbreaks under realistic public health scenarios.

Acknowledgements

I extend my deepest gratitude to Prof. Lin Wang and Prof. James Watmough for their invaluable guidance and support throughout this journey.

Special thanks to my wife, parents, siblings and close friends who have continuously been a source of unwavering support for all my endeavours.

Table of Contents

Abstract	ii
Acknowledgements	iii
Table of Contents	iv
List of Tables	vi
List of Figures	vii
1 Introduction	1
2 A Multi-strain SIARS Model	11
2.1 Model formulation	11
2.2 Existence of equilibria	17
2.3 Stability of equilibria	22
2.4 Numerical simulations and Discussions	29
3 A Multi-strain SVIARS model with masking	40
3.1 Model formulation	40
3.2 The disease-free equilibrium and basic reproduction number	46
3.3 Numerical simulations and discussions	51
3.4 Focused investigations for health-intervention related parameters	55
4 Conclusions and future work	63

Bibliography

71

Vita

List of Tables

- 2.1 Fixed parameter values used for simulations in the two-strain SIARS model. 34
- 3.1 Baseline health-intervention related parameter values used for simulations in the two-strain SVIARS model with masking. 54

List of Figures

2.1	A single-group multi-strain SIARS model	15
2.2	Illustration of strain-coexistence equilibria E^* for three strains.	23
2.3	Phase portrait illustrating stability of the strain 1 dominant equilibrium \hat{E}_1	36
2.4	Phase portrait showing convergence to the strain-1-dominant equilibrium \hat{E}_1 when $\mathcal{R}_{0,2} > 1$	37
2.5	Simulation of symptomatic infections in the neighbourhood of the infinite strain-coexistence equilibria E^* for two strains.	38
2.6	Equilibrium stability regions in $\mathcal{R}_{0,i}$ -space for the two-strain SIARS model.	39
3.1	A multi-strain SVIARS model with masking.	45
3.2	Phase portraits of symptomatic infections for strain 1 and strain 2 individuals in both unmasked (top) and masked groups (bottom).	59
3.3	Log-scale phase portraits illustrating the solutions of symptomatic infections for strain 1 and strain 2 individuals in both unmasked (top) and masked groups (bottom).	60
3.4	The influence of varying vaccine efficacy σ on the overall basic reproduction number \mathcal{R}_0	61
3.5	The overall basic reproduction number \mathcal{R}_0 as a function of the vaccination rate ψ_1 for unmasked individuals, with the vaccination rate for masked individuals fixed at six times ψ_1 , where $\psi_2 = 6\psi_1$	61

3.6	Contour plot showcasing variations of the overall basic reproduction number \mathcal{R}_0 as function of inward efficacy ϵ_{in} and outward efficacy ϵ_{out} of masks.	62
3.7	Contour plot of the overall basic reproduction number \mathcal{R}_0 illustrating its dependence on the migration rates ω_{12} (movement from the unmasked group to the masked group) and ω_{21} (movement from the masked group to the unmasked group).	62

Chapter 1

Introduction

In the recent past the world encountered a deadly virus known as Severe Acute Respiratory Syndrome Coronavirus 2 (SARS-CoV-2), more commonly known by the disease COVID-19, which left the world devastated by the influence it has on humans, economy and other social factors. According to the latest count by the World Health Organization (WHO) [37], the estimated reported cases have surpassed 777 million worldwide with over 7 million deaths.

The Centers for Disease Control and Prevention (CDC) [6] states when the first outbreak of COVID-19 happened on the 12th of December 2019, it was localized to only a minor cluster of patients in the city of Wuhan, Hubei Province, China. However, by the 13th of January 2020, the virus was detected by the Ministry of Health in Thailand and within a month it had spread to many countries and eventually classified as a pandemic on the 11th of March 2020, by WHO [11].

This is a great example of how volatile infectious diseases are and the scale to which they can develop. To avoid catastrophic end-results, preventive measures must be developed in time to effectively control the spread.

In this thesis we will only consider human to human transmission of a given infectious

disease; therefore, the implications that surround virus origins and crossing of the barrier from other species to humans are excluded. According to a review article by Zhou et al. [39], the transmission of diseases between humans occur primarily via air-dispersal of respiratory droplets. Other modes stated in the same article include aerosol transmission, fomite transmission and through body fluids; thus, we assume an averaged behaviour for the mentioned transmission methods in the models that will be developed in Chapter 2 and Chapter 3.

Disease transmission can be controlled by incorporating various non-pharmaceutical and pharmaceutical health interventions. A few examples of non-pharmaceutical methods include masks, gloves, social distancing, isolation, etc. Vaccines are generally considered the most prominent pharmaceutical intervention for controlling viral disease outbreaks; however, other methods include anti-inflammatory drugs, anticoagulants, etc.

In general, mathematical modelling has played a vital role in understanding the spread and control of infectious diseases. The analysis of mathematical models developed for predicting disease behaviours has enabled researchers and policymakers to gain insights into key epidemiological parameters (e.g., transmission rates, recovery rates, various thresholds above which there are disease outbreaks, etc.), and aids in evaluating strategies for disease control. Provided that all models have their unique characteristics, they have been evolved from the early works of Kermack and McKendrick [20] where a epidemic model of type-SIR was introduced that compartmentalizes the total population to three subpopulations namely **S**usceptible, **I**nfected and **R**ecovered.

Over the past few decades, there have been various use-cases for the standard SIR model by Kermack and McKendrick [20]. A review article by Lazebnik [21] details how the SIR model has been extended to various special cases that are distinguished

based on temporal and spatial extensions. Spatial extensions involve approaches that track disease spread across different geographic regions, and graph-based approaches model interactions represented through networks, such as infection graphs or location graphs. On the other hand, temporal extensions enrich the model by incorporating biological factors (e.g., **L**atency or **E**xposed stages as seen in SLIR/SEIR models), clinical distinctions (e.g., separating symptomatic and asymptomatic infections), sociological dynamics (e.g., mask-wearing behavior), and economic considerations (e.g., working vs. non-working states).

Some examples for diseases that have been studied using mathematical models are inclusive of COVID-19, Dengue, Malaria, etc. For the purposes of the literature review for this thesis, we focus on more recent studies published within the past five years. The case study of COVID-19 motivated the research conducted in this thesis; however, in addition to key papers that inspired the work in Chapter 2 and Chapter 3, we consider papers concerning other diseases to portray the scalability of mathematical models for predictive disease modelling.

A study by Contreras et al. [10] for COVID-19 in Santiago, Chile elaborates the development and analysis of an SEIARDQ model (i.e., **A** - asymptomatic infections, **D** - deceased individuals and **Q** - quarantined individuals) that investigates differences among social classes. The approach involved the compartmentalization of the total population into three different zones/patches, such that each zone had its own subpopulation (e.g., susceptible individuals from zones 1, 2 and 3). This method of population compartmentalization, due to varying characteristics among individuals, is referred to as multi-group modelling. Early studies by Nold [25] elaborate how multi-group modelling was developed.

In multi-group models, population heterogeneity is considered, where subpopulations of the total population are further categorized into distinct groups based on various

characteristics such as behavioural changes, demographics, etc. On the other hand, single-group modelling is the core component of compartmental models, where populations are considered to be homogeneous for a behavioural or non-behavioural trait. Furthermore, single-group models are created to provide an overall understanding about infectious disease behaviours and hence population heterogeneity is ignored. For example, a single group model would consider a population of individuals that have equal likelihood of being contracted with the disease and does not account for the varying levels of immunity for individuals.

The multi-group approach used in the paper by Contreras et al. [10], segments the groups based on social heterogeneity. However, health interventions were not considered. As a result, the study emphasizes the impact of enforcing mobility restrictions to contain outbreaks. Additionally, the study highlights the importance of tracking infectious individuals who do not display symptoms (i.e., asymptomatic) as they were found to be a major source of the disease outbreak through contact tracing.

A study by Rehman et al. [31] investigates a multi-group SEIR model for Malaria, incorporating important biological factors such as relapse and reinfection. Additionally, the model assumes homogeneous transmission dynamics within each group, without accounting for behavioural or clinical heterogeneity that may influence the spread of the disease.

Similarly, a study by Baude and Kimms [1] considering German epidemiological data for COVID-19 had formulated a multi-group SIRD model with nearby cities modelled as the groups. The model assumptions include a scenario where a pandemic had just begun, and pharmaceutical health interventions are not available. The results of the study portray that strategically timed lockdown measures effectively reduce the number of contacts made due to mobility between cities; thus, controlling the spread

of the disease and reducing overall costs associated to socioeconomic factors.

Another study by Ottaviano et al. [26] has no specific region of focus and formulates an SAIRS model, where the additional **S** at the end signifies that acquired immunity wanes and causes individuals to transition back to the susceptible population. The model includes the incorporation of vaccines as the only health intervention, and for any given population, the number of groups would correspond to the different communities based on factors such as ethnicity, age, gender, etc. The results of the study by Ottaviano et al. [26] highlight the controlled effects of vaccines on the number of infections produced.

A study performed by Gumel et al. [18] for COVID-19 in the USA, considers a model that incorporates masks and vaccines as health interventions. The behaviour of mask-wearing individuals was distinguished from those who do not, by segmenting every specific type of subpopulation into two different groups. The results of the study show different outcomes for varying levels of mask efficacy and vaccine efficacy.

A major limitation from the studies [1, 10, 18, 26] is that they had only considered the spread of one strain of COVID-19 for a given period of time; however, based on the epidemiological history of the disease, there have been multiple outbreaks related to various strains of the same virus.

Chronologically, there were three types of coronavirus that had caused severe outcomes in the past two decades. The first being Severe Acute Respiratory Syndrome Coronavirus (SARS-CoV) initially emerged from China in 2002, causing a global spread by 2003. The second being Middle-East Respiratory Syndrome Coronavirus (MERS-CoV) reported in 2012 in Saudi Arabia. The third and most recent being COVID-19 (SARS-CoV-2), deemed to be the most contagious, originated from Wuhan, Hubei Province, China in December 2019. Furthermore, for each disease, the virus evolves into newer types of strains. For example, in addition to the ances-

tral strain of COVID-19, a few emergent strains include Omicron, Delta and Alpha. Due to this reason, it not only advances viral replication but also increases the risk of recovered or vaccinated individuals becoming re-infected.

In contrast to the previous mention of multi-group modelling, there have been many studies that had used the alternative approach of developing single-group models [16, 22, 27, 30, 34] that consider the behaviour of multiple strains of a virus specific to an infectious disease and the effectiveness of various health interventions. While some interventions do work for a particular strain of a virus, they might not be as effective for emerging/newer strains. This approach is known as multi-strain modelling of infectious diseases.

A generic approach for mathematical modelling of multi-strain pandemics was studied by Lazebnik and Bunimovich-Mendrazitsky [34], specifically for an SIRD model. The study shows that an increase in the number of persisting strains within a population leads to an increase in the overall number of infections and a rise in the average disease-induced mortality rate. Provided the model discussed in the paper by Lazebnik and Bunimovich-Mendrazitsky [34] can be applied to any disease with multiple strains, no competition studies between strains were conducted to see the effects of one strain dominating or multiple strains coexisting. Further limitations of the model include the absence of waning immunity for recovered individuals and symptom-based separation of infected individuals.

The model formulations in this thesis were primarily inspired by the research of Gao et al. [16]. The model in the study by Gao et al. [16] portrays how various scenarios could exist when different strains compete to diminish one another or coexist. However, the model assumes asymptomatic infections must develop symptoms before recovering and hence excludes the direct conversion of asymptomatic infections to recovered individuals. Furthermore, factors such as waning immunity have not been

considered, and as a result, all recovered individuals attain complete immunity to all strains of a disease fitted into the model. These limitations are addressed in the model formulated in Chapter 2 in this thesis. The health intervention incorporated in the paper by Gao et al. [16] are masks, which are considered non-pharmaceutical. The method employed to investigate the effect of masks involved observing the result of the time-sensitive enforcement of mask mandates on the public. This aided in realizing that high disease-prevalence peaks can be prevented or delayed as a result of mask mandates enforced at critical points in time, as it greatly affects the emergence and frequency of subsequent COVID-19 waves.

As opposed to COVID-19, a single-group two-strain SIR model for Dengue fever was elaborated in a paper by Rashkov and Kooi [30]. The model considers the progression of the disease through sequential infections, where each individual is assumed to be infected by both strains consecutively. A rigorous analytical approach is employed to derive threshold conditions under which one strain can diminish the other, or both can coexist. Similarly, de Araújo et al. [12] extend this framework to a single-group four-strain model, offering a broader application of the multi-strain approach. However, both studies share certain limitations. Specifically, individuals who recover after being infected with all considered strains are assumed to acquire complete and lifelong immunity. Furthermore, the models do not incorporate waning immunity or symptom-based separation of infected individuals, which could lead to oversimplified dynamics compared to real-world transmission scenarios.

Another study by Massard et al. [22] showcases a single-group multi-strain model and uses COVID-19 data from France. The results imply that emergent strains at the time, namely: Alpha, Beta and Gamma, were deemed to be more transmissible than the original viral strain. This model considers the direct transition of susceptible individuals to both symptomatic and asymptomatic infections, and depicts a path for asymptomatic infections to recover without developing any symptoms. A similar

approach was incorporated in the multi-group single-strain study by Ottaviano et al. [26]. While the models in both referenced studies facilitated this separation, the model by Massard et al. [22] had not considered waning immunity for recovered individuals. Moreover, the study by Ottaviano et al. [26] does not consider the direct conversion of susceptible individuals to symptomatic infections and has not accounted for symptom-based separation of recovered individuals.

A study done by Otunuga [27] employs a single-group multi-strain model for COVID-19, distinguishing infected individuals by symptom status and considers vaccination as the sole intervention. Provided that factors such as waning immunity are included, recovered individuals are not tracked separately by whether or not they had displayed symptoms at the infectious stage. Consequently, asymptomatic and symptomatic infections merge into a single recovered compartment. Furthermore, the study also finds that vaccination reduces strain transmission but does not prevent the emergence of more transmissible variants. A key limitation is the lack of differentiation between asymptomatic infections that later develop symptoms and the absence of symptom-based tracking for the recovered populations.

Lastly, a paper by Campos et al. [5] formulated a single-group model for specifically three strains of COVID-19, considering only symptomatic infectious individuals and does not account for asymptomatic infections. However, a unique consideration in the paper by Campos et al. [5] is that vaccine booster shots were deemed to be the most effective measure of controlling COVID-19. For simplicity, the models constructed in this thesis will not factor in any effects of compounded immunity from one-time vaccination and re-vaccination.

Upon careful consideration of all prior-mentioned studies [1, 5, 10, 16, 18, 22, 26, 27], we lay the foundation upon which mathematical models are formulated in this thesis. Motivated by the referenced studies, the following research questions arise.

1. What are the outcomes for a generalized multi-strain SIARS model with the following considerations?
 - The fractional separation of susceptible to symptomatic and asymptomatic infections upon initial disease contraction, assuming asymptomatic individuals can still develop symptoms before they recover.
 - The distinction between recovered individuals from each strain based on whether they recover from symptomatic or asymptomatic infections, inclusive of variations in waning immunity for each case.

2. How can the model be extended to a multi-group multi-strain SIARS framework to address the following questions?
 - In the presence of multiple strains of a given infectious disease, how effective do masks and vaccines need to be, to control the overall spread of the disease?
 - How does compliance for mask mandates influence the overall spread of a given infectious disease?

To address these questions, in addition to early work by Kermack and McKendrick [20], compartmental modelling methods were incorporated from Brauer [3]. These models provide a general framework for studying the spread of infectious diseases and can be adapted to various pathogens, including viruses (e.g., coronaviruses, influenza), bacteria (e.g., tuberculosis), and other infectious agents. The flexibility of such models allows them to address fundamental epidemiological questions that apply across different types of communicable diseases.

The model (2.1.3) formulated in Chapter 2 provides insights for the first research question. As a result, the model (2.1.3) aims to provide greater flexibility for researchers studying similar research questions. Moreover, the model (3.1.3) in Chap-

ter 3 further extends model (2.1.3) to study the context described in the second research question. The formulation of both models in each chapter is followed by the respective analyses, accompanied by illustrations to convince the reader of the impact of the study conducted in this thesis. Finally, in Chapter 4, there will be a brief reflection of the findings from the models in Chapter 2 and Chapter 3, followed by a few suggestions for future work for any scholars referencing this thesis.

Chapter 2

A Multi-strain SIARS Model

Let the total population at time ‘ t ’ for a homogeneous group of individuals in a localized region be denoted by $N(t)$. This population is assumed to be coming in contact with multiple strains of a given communicable infectious disease.

Additionally, it is assumed that individuals have not yet received any external health interventions (e.g., masks, vaccines, etc.). Therefore, the immunity-related parameters introduced in this chapter will be based solely on naturally acquired immunity.

2.1 Model formulation

The subpopulations of the total population are compartmentalized based on the particular stages of the disease, i.e., susceptible, infected, and recovered, while considering the symptom-based separation of both infected and recovered individuals. Moreover, the model is of the form SIARS. The strain of the disease is referred to by the subscript i , where $i = 1, 2, \dots, n$ and n denotes the number of strains present in the population.

For a given point in time (t) the number of susceptible individuals is $S(t)$, the

number of strain- i symptomatic-infected individuals is $I_i(t)$, the number of strain- i asymptomatic-infected individuals is $A_i(t)$, the number of strain- i recovered individuals who had transitioned from $I_i(t)$ is $R_{I_i}(t)$ and the number of strain- i recovered individuals who had transitioned from $A_i(t)$ is $R_{A_i}(t)$. As a result, the total population can be expressed as

$$N(t) = S(t) + \sum_{i=1}^n [I_i(t) + A_i(t) + R_{I_i}(t) + R_{A_i}(t)]. \quad (2.1.1)$$

The recruitment of individuals into the susceptible population is given by the rate Λ (unit: persons/day), and the natural mortality rate μ (unit: 1/day) represents the frequency of deaths due to causes not related to the disease.

The transmission of infection is governed by an incidence function ϑ_i , which is referred as the force of infection that defines the rate at which susceptible individuals get infected by symptomatic infections or asymptomatic infections. Moreover, the transmission rates β_{I_i} and β_{A_i} (unit: 1/(persons · day)) represent the per capita risk of transmission per symptomatic or asymptomatic infected individual per day.

It is assumed that the number of effective contacts per individual does not change with population size. Therefore, we consider ϑ_i to be of a mass-action incidence formulation, which assumes that the rate of new infections is proportional to the product of susceptible and infectious individuals (for this reason, it is also referred to as bilinear incidence). The mass-action incidence approach was also followed in the main reference study by Gao et al. [16] that motivated the research elaborated in this chapter. Furthermore, the same assumption is seen in many other studies [15, 22, 27]. Another form of incidence is known as standard incidence, which is used in studies where disease transmission is population-density dependent, meaning that the per capita contact rate decreases as the population grows, and is used in cases

that model large populations [5, 8, 18]. Thus, ϑ_i is formulated as

$$\vartheta_i = \beta_{I_i} I_i + \beta_{A_i} A_i. \quad (2.1.2)$$

Susceptible individuals acquire infection with strain- i at a rate ϑ_i . A fraction θ_i of these individuals develop symptoms immediately upon infection, where $0 \leq \theta_i \leq 1$. The remaining individuals are initially asymptomatic and develop symptoms at the rate κ_{A_i} (unit: 1/day).

Symptomatic and asymptomatic infections recover at rates γ_{I_i} and γ_{A_i} (unit: 1/day) respectively. Meanwhile, disease-induced mortality occurs at rates δ_{I_i} and δ_{A_i} (unit: 1/day), representing the probability of death due to the disease per infected individual per day. Individuals in the symptom-based separated recovered populations lose their acquired immunity at rates η_{I_i} and η_{A_i} (unit: 1/day), transitioning back into the susceptible population.

For simplicity, it is assumed that individuals who had been infected with a particular strain loses their immunity completely when transitioning back to the susceptible population, implying that they are once again fully susceptible to all strains of a given infectious disease. Furthermore, for all strains $i = 1, 2, \dots, n$, the abbreviations $\xi_{I_i} = (\gamma_{I_i} + \delta_{I_i} + \mu)$ and $\xi_{A_i} = (\kappa_{A_i} + \gamma_{A_i} + \delta_{A_i} + \mu)$ represent a combination of parameters that imply the reciprocals $\frac{1}{\xi_{I_i}}$ and $\frac{1}{\xi_{A_i}}$ are the average times spent by infections in compartments I_i and A_i . Similarly, we consider $\xi_{R_{I_i}} = (\eta_{I_i} + \mu)$ and $\xi_{R_{A_i}} = (\eta_{A_i} + \mu)$, where the reciprocals $\frac{1}{\xi_{R_{I_i}}}$ and $\frac{1}{\xi_{R_{A_i}}}$ are the average times spent by recovered individuals in compartments R_{I_i} and R_{A_i} .

Therefore, for all strains $i = 1, 2, \dots, n$ the rate of change of the number of individuals in each subpopulation of the total population with respect to time is modelled by

system (2.1.3) as follows:

$$\begin{aligned}
\frac{dS}{dt} &= \Lambda - \sum_{i=1}^n \vartheta_i S + \sum_{i=1}^n (\eta_{I_i} R_{I_i} + \eta_{A_i} R_{A_i}) - \mu S, \\
\frac{dI_i}{dt} &= \theta_i \vartheta_i S + \kappa_{A_i} A_i - \xi_{I_i} I_i, \\
\frac{dA_i}{dt} &= (1 - \theta_i) \vartheta_i S - \xi_{A_i} A_i, \\
\frac{dR_{I_i}}{dt} &= \gamma_{I_i} I_i - \xi_{R_{I_i}} R_{I_i}, \\
\frac{dR_{A_i}}{dt} &= \gamma_{A_i} A_i - \xi_{R_{A_i}} R_{A_i}, \\
i &= 1, 2, \dots, n.
\end{aligned} \tag{2.1.3}$$

The solution of the system (2.1.3) is denoted by $(S, \mathbf{SV}_1, \mathbf{SV}_2, \dots, \mathbf{SV}_n) \in \mathbb{R}_+^{4n+1}$, where $\mathbf{SV}_i = [I_i, A_i, R_{I_i}, R_{A_i}]$ is a vector that contains the infected and recovered compartments for strain- i . The diagram that depicts system (2.1.3) is shown in Figure 2.1, and Theorem 2.1.1 confirms that model (2.1.3) admits unique, globally defined, and non-negative solutions.

Theorem 2.1.1. *For any given initial condition $(S(0), \mathbf{SV}_1(0), \mathbf{SV}_2(0), \dots, \mathbf{SV}_n(0)) \in \mathbb{R}_+^{4n+1}$, there exists a unique solution to model (2.1.3) which exists globally, remains non-negative and is bounded.*

Proof. Note that the functions on the right-hand side of model (2.1.3) are continuously differentiable. It follows from the Fundamental Existence-Uniqueness Theorem [29] that model (2.1.3) admits a unique solution on $[0, \tau)$ for some $\tau > 0$.

For any given initial condition $(S(0), \mathbf{SV}_1(0), \mathbf{SV}_2(0), \dots, \mathbf{SV}_n(0)) \in \mathbb{R}_+^{4n+1}$, we next show that the solution remains non-negative for $t > 0$. By continuity of solutions, any solution that is initially non-negative and becomes negative in one or more components must occur on the boundary of \mathbb{R}_+^{4n+1} at some time. Without loss of generality, we assume the initial condition is on the boundary of \mathbb{R}_+^{4n+1} .

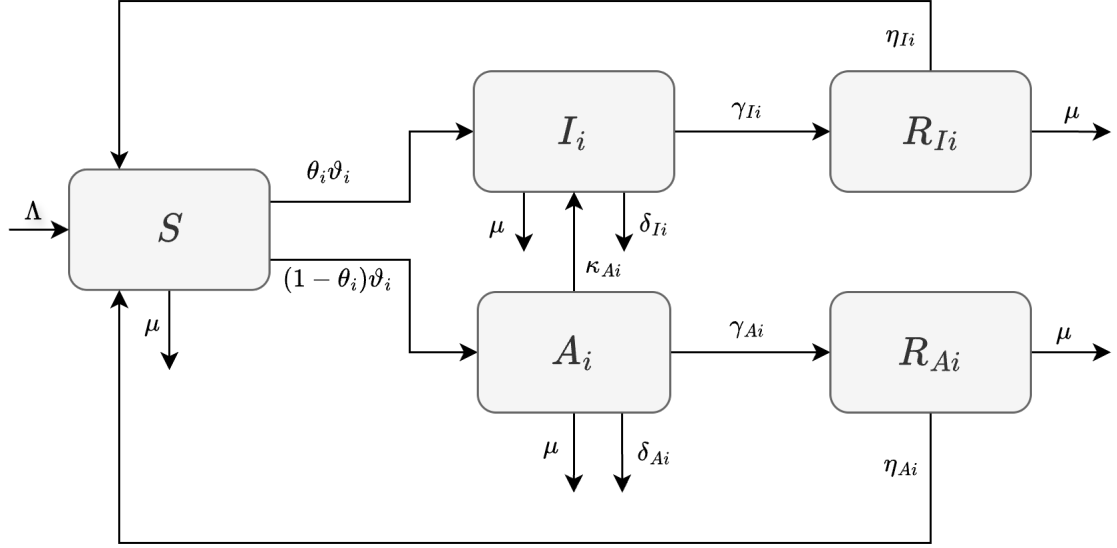


Figure 2.1: A single-group multi-strain SIARS model. New individuals enter the susceptible compartment at a rate Λ , with a natural mortality rate μ across all compartments, except for disease-induced mortality δ_{I_i} and δ_{A_i} in infectious states. A fraction θ_i of susceptible individuals transition to symptomatic (I_i) and the remaining portion $(1 - \theta_i)$ transitions to asymptomatic (A_i) infections at rate ϑ_i . Asymptomatic individuals can develop symptoms at a rate κ_{A_i} . Recovery occurs at rates γ_{I_i} and γ_{A_i} , leading to respective recovered compartments (R_{I_i} and R_{A_i}). Immunity wanes at rates η_{I_i} and η_{A_i} , transitioning individuals back to the susceptible compartment.

On the S -boundary ($S = 0, \mathbf{S}\mathbf{V}_i \geq 0, i = 1, 2, \dots, n$), we have

$$\left. \frac{dS}{dt} \right|_{S=0} = \Lambda + \sum_{i=1}^n (\eta_{I_i} R_{I_i} + \eta_{A_i} R_{A_i}) > 0,$$

which implies that $S(t)$ cannot become negative.

Next, we show that $I_i(t)$ and $A_i(t)$ cannot become negative. On the I_i -boundary ($I_i = 0, S \geq 0, A_i \geq 0, R_{I_i} \geq 0, R_{A_i} \geq 0, i = 1, 2, \dots, n$), we have

$$\left. \frac{dI_i}{dt} \right|_{I_i=0} = \theta_i \beta_{A_i} A_i S + \kappa_{A_i} A_i \geq 0,$$

and the equality occurs if and only if $I_i = A_i = 0$. Similarly, on the A_i -boundary

$(A_i = 0, S \geq 0, I_i \geq 0, R_{I_i} \geq 0, R_{A_i} \geq 0, i = 1, 2, \dots, n)$, we have

$$\left. \frac{dA_i}{dt} \right|_{A_i=0} = (1 - \theta_i)\beta_{I_i}I_i S \geq 0,$$

and the equality occurs if $I_i = A_i = 0$. It follows from the second and third equations of system (2.1.3) that $I_i = A_i = 0$ is invariant. Therefore, by uniqueness of solutions, the solutions to the sub-system containing equations two and three from (2.1.3) cannot become negative.

From the fourth equation of system (2.1.3) we have

$$R_{I_i}(t) = R_{I_i}(0)e^{-\xi_{R_{I_i}}t} + \int_0^t \gamma_{I_i}I_i(\tau)e^{-\xi_{R_{I_i}}(t-\tau)}d\tau.$$

With any given non-negative initial condition, the only way $R_{I_i}(t)$ can become negative is if the integral is negative, which implies $I_i(t)$ becomes negative before $R_{I_i}(t)$. Since $I_i(t)$ is non-negative, it follows that $R_{I_i}(t) \geq 0$ for all $t \geq 0$.

Moreover, from the fifth equation of system (2.1.3) we have

$$R_{A_i}(t) = R_{A_i}(0)e^{-\xi_{R_{A_i}}t} + \int_0^t \gamma_{A_i}A_i(\tau)e^{-\xi_{R_{A_i}}(t-\tau)}d\tau.$$

The integral in the solution implies that $A_i(t)$ becomes negative before $R_{A_i}(t)$. Since $A_i(t)$ is non-negative, we conclude that $R_{A_i}(t) \geq 0$ for all $t \geq 0$.

Next, we show the solution $(S, \mathbf{SV}_1, \mathbf{SV}_2, \dots, \mathbf{SV}_n) \in \mathbb{R}_+^{4n+1}$ is bounded. Note that

$$\frac{dN}{dt} = \Lambda - \mu N - \sum_{i=1}^n (\delta_{I_i}I_i + \delta_{A_i}A_i).$$

It follows from the non-negativity of the solution that

$$\frac{dN}{dt} \leq \Lambda - \mu N, \tag{2.1.4}$$

which yields

$$N(t) \leq \frac{\Lambda}{\mu} + \left(N(0) - \frac{\Lambda}{\mu} \right) e^{-\mu t}.$$

Thus,

$$N(t) \leq \max \left(N(0), \frac{\Lambda}{\mu} \right),$$

and

$$\limsup_{t \rightarrow \infty} N(t) \leq \frac{\Lambda}{\mu}.$$

Therefore, the solution is bounded and hence exists globally. \square

Remark. *If $\theta_i = \eta_{Ii} = \eta_{Ai} = 0$ for strains $i = 1, 2, \dots, n$, then susceptible individuals will not immediately develop symptoms upon acquiring the infection and there will be no waning immunity for recovered individuals. For such a case, the model (2.1.3) reduces to the main reference model by Gao et al. [16]. On the other hand, if $\theta_i = 1$ there would be no asymptomatic infections created and the model reduces to a multi-strain SIRS model.*

2.2 Existence of equilibria

Compartmental models of infectious diseases described by systems of ODEs are essentially dynamical systems. A big part of most analyses related to dynamical systems is to find various scenarios, where the system will have steady-state solutions classified as equilibrium points. Therefore, in this section, we examine the existence of all possible equilibria for model (2.1.3).

Before presenting the theorem that characterizes all possible equilibria in model (2.1.3), we introduce an important threshold parameter, denoted by $\mathcal{R}_{0,i}$, which depends on parameters specifically related to strain- i , and is given by

$$\mathcal{R}_{0,i} = \left(\frac{[\theta_i \xi_{Ai} + (1 - \theta_i) \kappa_{Ai}] \beta_{Ii}}{\xi_{Ii} \xi_{Ai}} + \frac{(1 - \theta_i) \beta_{Ai}}{\xi_{Ai}} \right) \frac{\Lambda}{\mu}, \quad (2.2.1)$$

$$i = 1, 2, \dots, n.$$

Theorem 2.2.1. *System (2.1.3) admits multiple equilibria, which can be classified into the following three categories:*

(a) **Disease-Free Equilibrium (DFE):** *There exists exactly one unique DFE denoted by:*

$$E_0 = (S_0, \mathbf{SV}_1, \mathbf{SV}_2, \dots, \mathbf{SV}_n) \in \mathbb{R}_+^{4n+1},$$

where

$$S_0 = \frac{\Lambda}{\mu}, \mathbf{SV}_i = \mathbf{0}_{4 \times 1}, \forall i \in \{1, 2, \dots, n\}.$$

(b) **Strain-Dominant Equilibria:** *If $\mathcal{R}_{0,i} > 1$, there exists the strain-dominant equilibrium denoted by:*

$$\hat{E}_i = (\hat{S}_i, \mathbf{SV}_1, \mathbf{SV}_2, \dots, \mathbf{SV}_n) \in \mathbb{R}_+^{4n+1},$$

where

$$\hat{S}_i = \frac{\Lambda}{\mu} \left(\frac{1}{\mathcal{R}_{0,i}} \right), \mathbf{SV}_j = \begin{cases} [\hat{I}_i, \hat{A}_i, \hat{R}_{Ii}, \hat{R}_{Ai}], & \text{if } j = i, \\ \mathbf{0}_{4 \times 1}, & \text{if } j \neq i \end{cases}$$

with

$$\hat{I}_i = \frac{\Lambda}{z_i} \left(1 - \frac{1}{\mathcal{R}_{0,i}} \right), \hat{A}_i = \left(\frac{(1 - \theta_i) \xi_{Ii}}{\theta_i \xi_{Ai} + (1 - \theta_i) \kappa_{Ai}} \right) \hat{I}_i,$$

$$\hat{R}_{Ii} = \left(\frac{\gamma_{Ii}}{\xi_{RIi}} \right) \hat{I}_i, \hat{R}_{Ai} = \left(\frac{\gamma_{Ai}}{\xi_{RAi}} \right) \hat{A}_i,$$

in which

$$z_i = \frac{z_{ia}}{z_{ib}},$$

where

$$\begin{aligned}
z_{ia} &= \theta_i \xi_{RAi} \xi_{Ai} \left(\eta_{Ii} (\delta_{Ii} + \mu) + \mu \xi_{Ii} \right) + (1 - \theta_i) \left(\xi_{RIi} \xi_{RAi} \left[\xi_{Ii} (\delta_{Ai} + \mu) \right. \right. \\
&\quad \left. \left. + \kappa_{Ai} (\delta_{Ii} + \mu) \right] + \mu \gamma_{Ai} \xi_{RIi} \xi_{Ii} + \mu \gamma_{Ii} \kappa_{Ai} \xi_{RAi} \right), \\
z_{ib} &= \xi_{RIi} \xi_{RAi} \left(\theta_i \xi_{Ai} + (1 - \theta_i) \kappa_{Ai} \right).
\end{aligned}$$

(c) **Strain-Coexistence Equilibria:** Let $\mathcal{J} \subseteq \{1, 2, \dots, n\}$ with $|\mathcal{J}| \geq 2$. Suppose the basic reproduction numbers $\mathcal{R}_{0,j}$ are all equal for $j \in \mathcal{J}$,

$$\mathcal{R}_{0,j} = \mathcal{R}_0^* > 1, \forall j \in \mathcal{J}.$$

Then, the system (2.1.3) admits infinitely many equilibria corresponding to the coexistence of all strains in \mathcal{J} . The equilibrium is represented by:

$$E^* = (S^*, \mathbf{SV}_1, \mathbf{SV}_2, \dots, \mathbf{SV}_n) \in \mathbb{R}_+^{4n+1},$$

where the state vector \mathbf{SV}_i for each strain- i takes the form:

$$\mathbf{SV}_j = \begin{cases} [I_j^*, A_j^*, R_{Ij}^*, R_{Aj}^*], & \text{if } j \in \mathcal{J}, \\ \mathbf{0}_{4 \times 1}, & \text{if } j \notin \mathcal{J}. \end{cases}$$

The susceptible population at the equilibrium is:

$$S^* = \frac{\Lambda}{\mu} \left(\frac{1}{\mathcal{R}_0^*} \right).$$

For each coexisting strain $j \in \mathcal{J}$, the equilibrium components are given by:

$$I_j^* = \frac{\Lambda}{z_j} \left(1 - \frac{1}{\mathcal{R}_0^*} \right), \quad A_j^* = \left(\frac{(1 - \theta_j) \xi_{Ij}}{\theta_j \xi_{Aj} + (1 - \theta_j) \kappa_{Aj}} \right) I_j^*,$$

$$R_{I_j}^* = \left(\frac{\gamma_{I_j}}{\xi_{RI_j}} \right) I_j^*, \quad R_{A_j}^* = \left(\frac{\gamma_{A_j}}{\xi_{RA_j}} \right) A_j^*.$$

The values of I_j^* satisfy the following equilibrium condition:

$$\sum_{j \in \mathcal{J}} z_j I_j^* = \Lambda \left(1 - \frac{1}{\mathcal{R}_0^*} \right),$$

where $I_j^* \in (0, \hat{I}_j)$ and z_j has an identical form to z_i defined earlier in case (b) for strain-dominant equilibria.

Proof. Equilibrium points for the system (2.1.3) represent scenarios that provide insights into whether a disease persists or eventually dies out. Therefore, to investigate all possible equilibria, we equate the derivatives of all state variables in system (2.1.3) to zero.

$$0 = \Lambda - \sum_{i=1}^n \vartheta_i S + \sum_{i=1}^n (\eta_{I_i} R_{I_i} + \eta_{A_i} R_{A_i}) - \mu S \quad (2.2.2)$$

$$0 = \theta_i \vartheta_i S + \kappa_{A_i} A_i - \xi_{I_i} I_i \quad (2.2.3)$$

$$0 = (1 - \theta_i) \vartheta_i S - \xi_{A_i} A_i \quad (2.2.4)$$

$$0 = \gamma_{I_i} I_i - \xi_{RI_i} R_{I_i} \quad (2.2.5)$$

$$0 = \gamma_{A_i} A_i - \xi_{RA_i} R_{A_i} \quad (2.2.6)$$

From equations (2.2.5) and (2.2.6) we form linear relationships for the recovered compartments, where

$$R_{I_i} = \left(\frac{\gamma_{I_i}}{\xi_{RI_i}} \right) I_i, \quad R_{A_i} = \left(\frac{\gamma_{A_i}}{\xi_{RA_i}} \right) A_i, \quad \forall i = 1, 2, \dots, n. \quad (2.2.7)$$

The equation (2.2.4) can be written as

$$\vartheta_i S = \left(\frac{\xi_{A_i}}{1 - \theta_i} \right) A_i. \quad (2.2.8)$$

Substituting (2.2.8) into equation (2.2.3) and solving for A_i results in a linear relationship between A_i and I_i as follows:

$$A_i = \left(\frac{(1 - \theta_i)\xi_{I_i}}{\theta_i\xi_{A_i} + (1 - \theta_i)\kappa_{A_i}} \right) I_i, \forall i = 1, 2, \dots, n. \quad (2.2.9)$$

Recalling ϑ_i from equation (2.1.2) and substituting (2.2.9) into equation (2.2.3), we obtain

$$(S - S_i)I_i = 0, \quad (2.2.10)$$

where

$$S_i = \frac{\xi_{I_i}\xi_{A_i}}{\beta_{I_i}[\theta_i\xi_{A_i} + (1 - \theta_i)\kappa_{A_i}] + \beta_{A_i}\xi_{I_i}(1 - \theta_i)}. \quad (2.2.11)$$

Equation (2.2.10) implies that

$$\text{either } I_i = 0, \text{ or } S = S_i.$$

Expressing S_i in terms of $\mathcal{R}_{0,i}$, we obtain:

$$S_i = \frac{\Lambda}{\mu} \left(\frac{1}{\mathcal{R}_{0,i}} \right). \quad (2.2.12)$$

The solution $I_i = 0$ of (2.2.10) represents the disease-free equilibrium (DFE) E_0 as stated in the theorem because, when this solution is substituted to equations (2.2.7) and (2.2.9), it results in zero solutions. However, to evaluate the value for the susceptible compartment, we consider equation (2.2.2) that yields the solution $S = S_0$ as stated in the theorem.

For the case of the second solution $S = S_i$ when $I_i \neq 0$; the solutions (2.2.12), (2.2.7) and (2.2.9) are substituted into equation (2.2.2) that yield the solutions for $I_i = \hat{I}_i$ and $I_i = I_j^*$ for cases (b) and (c) stated in the theorem. The remaining solutions

for the susceptible individuals, asymptomatic infections, and recovered individuals stated in the theorem can be obtained for both equilibria cases (b) and (c) using the equations (2.2.12),(2.2.9) and (2.2.7).

For the case of a strain- i dominant equilibrium \hat{E}_i , we have $\hat{I}_i > 0$, and the right-hand side of the expression for \hat{I}_i is positive only when $\mathcal{R}_{0,i} > 1$, making it the condition necessary for the existence of \hat{E}_i . We can further extend this relation for the strain-coexistence equilibria E^* , for which we have $I_j^* > 0$; thus, the condition $\mathcal{R}_{0,j} = \mathcal{R}_0^* > 1$ must be satisfied for the right-hand side of the linear expression for I_j^* to be positive.

Another interesting implication is that $I_j^* \in (0, \hat{I}_j)$ as stated in the theorem, and is illustrated in Figure 2.2. The reason for the boundary points to be equal to the number of symptomatic infections of a strain dominant equilibrium is due to the diminishing of symptomatic infections of all other competing strains. \square

2.3 Stability of equilibria

The stability of an equilibrium is assessed by examining the behaviour of perturbed solutions. If solutions remain close to an equilibrium it is referred to as ‘Lyapunov Stable’; however, if solutions converge to an equilibrium, it is known as ‘Asymptotically Stable’. Conversely, if solutions diverge, the equilibrium is unstable.

In this thesis, we focus on local asymptotic stability (LAS). Establishing conditions for global stability remains an open problem for multi-strain models such as (2.1.3), primarily due to the lack of a general methodology for constructing Lyapunov functions that provide global stability insights. While simpler models such as those studied by Gao et al.[16], have well-defined Lyapunov functions, they typically do not account for waning immunity. However, in model (2.1.3), waning immunity leads

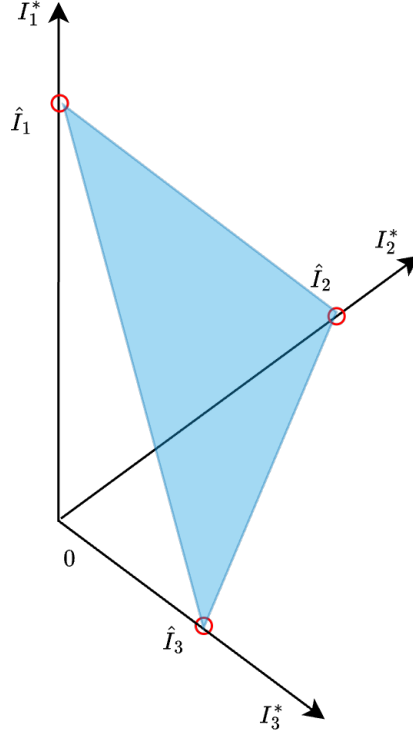


Figure 2.2: Illustration of strain-coexistence equilibria E^* for three strains. The figure shows a three-dimensional illustration of the infinite number of equilibria represented by the blue plane connecting the number of symptomatic infections for three strain dominant equilibria \hat{I}_i for $i = 1, 2, 3$ represented by the open red circles. The circles being open indicate that the boundaries exclude the strain-coexistence equilibria values I_j^* for $j = 1, 2, 3$.

to recovered individuals returning to the susceptible population, which introduces an additional complexity in constructing Lyapunov functions.

Following the existence of the DFE stated in theorem 2.2.1, we use the next generation matrix method introduced by Watmough and van den Driessche [35] to derive the basic reproduction number for model (2.1.3). The basic reproduction number can be defined as the number of secondary infections produced by one infectious individual in a fully susceptible population.

The system (2.1.3) is rewritten in the form $\dot{\mathbf{X}} = \mathcal{F} - \mathcal{V}$, where \mathbf{X} is a vector and it is of the form $\mathbf{X} = [I_1 \ A_1 \ I_2 \ A_2 \ \dots \ I_n \ A_n]^T$. The vector \mathcal{F} is called the ‘Vector of New

Infections' and it represents the expected number of secondary infections produced by individuals in the infectious subpopulations in vector \mathbf{X} . Moreover, the vector \mathcal{V} is known as the 'Vector of Transitions' and it represents the outflow of individuals from the infectious subpopulations in vector \mathbf{X} . Thus, we have the vectors

$$\mathcal{F} = \begin{pmatrix} \theta_1 \vartheta_1 S \\ (1 - \theta_1) \vartheta_1 S \\ \vdots \\ \theta_n \vartheta_n S \\ (1 - \theta_n) \vartheta_n S \end{pmatrix}, \quad \mathcal{V} = \begin{pmatrix} \xi_{I_1} I_1 - \kappa_{A_1} A_1 \\ \xi_{A_1} A_1 \\ \vdots \\ \xi_{I_n} I_n - \kappa_{A_n} A_n \\ \xi_{A_n} A_n \end{pmatrix},$$

and using the two vectors \mathcal{F} and \mathcal{V} , we evaluate the matrix of new infections \mathbf{F} and the matrix of transitions \mathbf{V} , where $\mathbf{F} = \frac{\partial \mathcal{F}}{\partial \mathbf{X}}$ and $\mathbf{V} = \frac{\partial \mathcal{V}}{\partial \mathbf{X}}$. Moreover, $S = S_0 = \frac{\Lambda}{\mu}$ is substituted to the matrix \mathbf{F} which yields,

$$\mathbf{F} = \begin{pmatrix} \frac{\theta_1 \beta_{I_1} \Lambda}{\mu} & \frac{\theta_1 \beta_{A_1} \Lambda}{\mu} & \dots & 0 & 0 \\ \frac{(1-\theta_1) \beta_{I_1} \Lambda}{\mu} & \frac{(1-\theta_1) \beta_{A_1} \Lambda}{\mu} & \dots & 0 & 0 \\ \vdots & \vdots & \ddots & \vdots & \vdots \\ 0 & 0 & \dots & \frac{\theta_n \beta_{I_n} \Lambda}{\mu} & \frac{\theta_n \beta_{A_n} \Lambda}{\mu} \\ 0 & 0 & \dots & \frac{(1-\theta_n) \beta_{I_n} \Lambda}{\mu} & \frac{(1-\theta_n) \beta_{A_n} \Lambda}{\mu} \end{pmatrix},$$

and

$$\mathbf{V} = \begin{pmatrix} \xi_{I_1} & -\kappa_{A_1} & \dots & 0 & 0 \\ 0 & \xi_{A_1} & \dots & 0 & 0 \\ \vdots & \vdots & \ddots & \vdots & \vdots \\ 0 & 0 & \dots & \xi_{I_n} & -\kappa_{A_n} \\ 0 & 0 & \dots & 0 & \xi_{A_n} \end{pmatrix}.$$

The next-generation matrix is \mathbf{G} , where $\mathbf{G} = \mathbf{FV}^{-1}$. Evaluating the next-generation

matrix \mathbf{G} results in

$$\mathbf{G} = \begin{pmatrix} \mathbf{G}_1 & \dots & 0 \\ \vdots & \ddots & \vdots \\ 0 & \dots & \mathbf{G}_n \end{pmatrix}.$$

The sub-matrices $\mathbf{G}_i \in \mathbb{R}^{2 \times 2}$ correspond to each strain $i = 1, 2, \dots, n$, and are expressed as an inner product of two vectors, such that

$$\mathbf{G}_i = \mathbf{c}^T \mathbf{g}_i,$$

where

$$\mathbf{g}_i = \left(\frac{\theta_i \beta_{Ii} \Lambda}{\xi_{Ii} \mu} \quad \frac{\theta_i \Lambda}{\xi_{Ai} \mu} \left(\frac{\beta_{Ii} \kappa_{Ai}}{\xi_{Ii}} + \beta_{Ai} \right) \right), \text{ and } \mathbf{c} = \left(1 \quad \frac{1 - \theta_i}{\theta_i} \right).$$

Moreover, the zeros on the off-diagonals of the next-gen matrix \mathbf{G} form triangular null matrices. It can be noted that the matrices \mathbf{G}_i are all rank 1; therefore, of the two eigenvalues, one is non-zero and the other is zero. The non-zero eigenvalue ζ_i is the trace of matrix \mathbf{G}_i , where

$$\zeta_i = \text{tr}(\mathbf{G}_i) = \mathbf{g}_i \mathbf{c}^T,$$

and

$$\zeta_i = \left(\frac{[\theta_i \xi_{Ai} + (1 - \theta_i) \kappa_{Ai}] \beta_{Ii}}{\xi_{Ii} \xi_{Ai}} + \frac{(1 - \theta_i) \beta_{Ai}}{\xi_{Ai}} \right) \frac{\Lambda}{\mu}.$$

The eigenvalue ζ_i consists of parameters exclusive to strain- i ; hence, we represent each non-zero eigenvalue of the next generation matrix \mathbf{G} as the basic reproduction number of each individual strain, which is exactly the same form for the threshold $\mathcal{R}_{0,i}$ introduced earlier in equation (2.2.1). The overall basic reproduction number \mathcal{R}_0 for system (2.1.3) is the spectral radius of matrix \mathbf{G} , where

$$\mathcal{R}_0 = \rho(\mathbf{G}) = \max\{\mathcal{R}_{0,i}\}, \forall i = 1, 2, \dots, n.$$

Furthermore, we have the following theorem that describes the local stability of the DFE and is based on the works by Watmough and van den Driessche [35].

Theorem 2.3.1. *When $\mathcal{R}_0 < 1$ the DFE E_0 is locally asymptotically stable (LAS). Conversely, when $\mathcal{R}_0 > 1$, E_0 is unstable.*

To analyze the local asymptotic stability of a strain-dominant equilibrium \hat{E}_i , we re-write system (2.1.3) in the form $\frac{d\Gamma}{dt} = \mathbf{K}(\Gamma)$, where $\Gamma = [S \ I_1 \ A_1 \ R_{I1} \ R_{A1} \ \dots \ I_n \ A_n \ R_{In} \ R_{An}]^T \in \mathbb{R}_+^{(4n+1) \times 1}$ is a vector that contains all state variables. Without loss of generality we assume that the dominant strain $i = 1$; thus, the Jacobian matrix \mathbb{J} of system (2.1.3) evaluated at \hat{E}_1 is

$$\mathbb{J}\Big|_{\hat{E}_1} = \begin{pmatrix} \mathbb{J}_1 & \bar{\mathbb{J}}_2 & \cdots & \bar{\mathbb{J}}_n \\ \mathbf{0} & \mathbb{J}_2 & \cdots & 0 \\ \vdots & \vdots & \ddots & \vdots \\ \mathbf{0} & 0 & \cdots & \mathbb{J}_n \end{pmatrix} \in \mathbb{R}^{(4n+1) \times (4n+1)}, \quad (2.3.1)$$

where $\mathbf{0}_{5 \times 5}$ are 5-dimensional zero matrices, and the other zeros form triangular null matrices on the off-diagonals. From the Jacobian matrix (2.3.1) we have the sub-matrix $\mathbb{J}_1 \in \mathbb{R}^{5 \times 5}$ that includes terms exclusive to strain 1, where

$$\mathbb{J}_1 = \begin{pmatrix} -(\hat{\vartheta}_1 + \mu) & -\beta_{I1}\hat{S}_1 & -\beta_{A1}\hat{S}_1 & \eta_{I1} & \eta_{A1} \\ \theta_1\hat{\vartheta}_1 & \theta_1\beta_{I1}\hat{S}_1 - \xi_{I1} & \theta_1\beta_{A1}\hat{S}_1 + \kappa_{A1} & 0 & 0 \\ (1 - \theta_1)\hat{\vartheta}_1 & (1 - \theta_1)\beta_{I1}\hat{S}_1 & (1 - \theta_1)\beta_{A1}\hat{S}_1 - \xi_{A1} & 0 & 0 \\ 0 & \gamma_{I1} & 0 & -\xi_{RI1} & 0 \\ 0 & 0 & \gamma_{A1} & 0 & -\xi_{RA1} \end{pmatrix}. \quad (2.3.2)$$

The term $\hat{v}_1 = \beta_{I1}\hat{I}_1 + \beta_{A1}\hat{A}_1$ refers to the force of infection from (2.1.2) when evaluated at \hat{E}_1 . Furthermore, we have two other combinations of sub-matrices in (2.3.1) corresponding to all other strains $j = 2, 3, \dots, n$ described by

$$\mathbb{J}_j = \begin{pmatrix} \theta_j\beta_{Ij}\hat{S}_1 - \xi_{Ij} & \theta_j\beta_{Aj}\hat{S}_1 + \kappa_{Aj} & 0 & 0 \\ (1 - \theta_j)\beta_{Ij}\hat{S}_1 & (1 - \theta_j)\beta_{Aj}\hat{S}_1 - \xi_{Aj} & 0 & 0 \\ \gamma_{Ij} & 0 & -\xi_{RIj} & 0 \\ 0 & \gamma_{Aj} & 0 & -\xi_{RAj} \end{pmatrix} \quad (2.3.3)$$

and

$$\bar{\mathbb{J}}_j = \begin{pmatrix} \bar{\mathbb{J}}_{j,1} \\ \mathbf{0} \end{pmatrix},$$

where

$$\bar{\mathbb{J}}_{j,1} = \begin{pmatrix} -\beta_{Ij}\hat{S}_1 & -\beta_{Aj}\hat{S}_1 & \eta_{Ij} & \eta_{Aj} \end{pmatrix} \in \mathbb{R}_+^{1 \times 4},$$

and $\mathbf{0}_{4 \times 4}$ are 4-dimensional zero matrices.

Theorem 2.3.2. *For system (2.1.3), the strain-dominant equilibrium \hat{E}_1 is LAS if and only if the two following conditions are satisfied.*

1. All eigenvalues of the sub-matrix \mathbb{J}_1 in (2.3.2) have negative real parts.
2. $\mathcal{R}_{0,1} > 1$ and $\mathcal{R}_{0,1} > \mathcal{R}_{0,j} \forall j = 2, 3, \dots, n$.

Proof. The characteristic polynomial that includes insights about the eigenvalues (λ) of the Jacobian matrix (2.3.1) is of the form

$$\sum_{k=0}^5 (a_{i,k}\lambda^k) \prod_{j \neq i}^{n-1} \left[(\lambda + (\eta_{Ij} + \mu)) (\lambda + (\eta_{Aj} + \mu)) \sum_{k=0}^2 (a_{j,k}\lambda^k) \right] = 0, \quad (2.3.4)$$

where $i = 1$ and $j = 2, 3, \dots, n$. Moreover, the coefficients $a_{i,5} = a_{j,2} = 1$.

It can be noted that the first fifth-order characteristic polynomial in (2.3.4) emerges from matrix \mathbb{J}_1 defined in (2.3.2) for the dominant strain 1, which implies the first five-dimensional subspace is unique to the dominant strain; thus, the eigenvalues $\lambda_1, \lambda_2, \dots, \lambda_5$ of matrix \mathbb{J}_1 should all have negative real parts and is mentioned in the first condition for local asymptotic stability in Theorem 2.3.2. The remaining eigenvalues emerge from the matrices \mathbb{J}_j in (2.3.3) and form triples of factors that contain a pair of fully-factorized strictly negative eigenvalues

$$\lambda_{j,1} = -(\eta_{Ij} + \mu) \text{ and } \lambda_{j,2} = -(\eta_{Aj} + \mu),$$

with the remaining factor being a second-order polynomial $\lambda^2 + a_{j,1}\lambda + a_{j,0} = 0$ that contains information about the other two eigenvalues $\lambda_{j,3}$ and $\lambda_{j,4}$.

From the quadratic formula we have

$$\lambda_{j,3} = \frac{-a_{j,1} + \sqrt{a_{j,1}^2 - 4a_{j,0}}}{2} \text{ and } \lambda_{j,4} = \frac{-a_{j,1} - \sqrt{a_{j,1}^2 - 4a_{j,0}}}{2}.$$

To achieve local stability we must have eigenvalues with negative real parts, which would be satisfied if $a_{j,1} > 0$. Moreover, the functional form of $a_{j,1}$ is

$$a_{j,1} = \xi_{Ij} - \theta_j \beta_{Ij} \left(\frac{1}{\mathcal{R}_{0,1}} \right) \frac{\Lambda}{\mu} + \xi_{Aj} - (1 - \theta_j) \beta_{Aj} \left(\frac{1}{\mathcal{R}_{0,1}} \right) \frac{\Lambda}{\mu}. \quad (2.3.5)$$

For all other strains (i.e., $j = 2, 3, \dots, n$), we have the basic reproduction number $\mathcal{R}_{0,j}$ from (2.2.1); thus, we can simplify (2.3.5) to obtain

$$\begin{aligned} a_{j,1} = & \xi_{Ij} \left(1 - \frac{\mathcal{R}_{0,j}}{\mathcal{R}_{0,1}} \right) + \xi_{Aj} \left(1 - \frac{\mathcal{R}_{0,j}}{\mathcal{R}_{0,1}} \right) + \left[\left(\frac{1}{\xi_{Aj}} + \frac{1}{\xi_{Ij}} \right) (1 - \theta_j) \kappa_{Aj} \beta_{Ij} \right. \\ & \left. + \left(\frac{\theta_j \xi_{Aj} \beta_{Ij}}{\xi_{Ij}} + \frac{(1 - \theta_j) \xi_{Ij} \beta_{Aj}}{\xi_{Aj}} \right) \right] \left(\frac{1}{\mathcal{R}_{0,1}} \right) \frac{\Lambda}{\mu}. \end{aligned}$$

The result implies that for both cases $\mathcal{R}_{0,j} > 1$ and $\mathcal{R}_{0,j} < 1$, the sufficient condition $\mathcal{R}_{0,1} > \mathcal{R}_{0,j}$ ensures $a_{j,1} > 0$; hence, the second condition in Theorem 2.3.2 is proved.

□

The local stability of strain-coexistence equilibria $E_{\mathcal{J}}^*$ stated in Theorem 2.2.1 remains inconclusive from the linearization of system (2.1.3). However, Figure 2.5 illustrates a simulation performed to observe the behaviour of solutions to system (2.1.3) in the context of two strains coexisting, and will be discussed further in Section 2.4.

2.4 Numerical simulations and Discussions

For simplicity, the simulations and discussions done in this section will be limited to a two-strain SIARS model, where system (2.1.3) has been simplified for the case of $i = 1, 2$. The two strains considered in this section are theoretical constructs used purely for illustrative purposes. Moreover, strain 1 is assumed to be more infectious than strain 2.

To investigate behaviours associated with all types of equilibria introduced in Theorem 2.2.1, we find parameter values that satisfy the analytical results introduced in Theorem 2.2.1, 2.3.1, and 2.3.2. The parameter values in Table 2.1 are informed by previous studies and reflect the rationale for each value. Provided these values are approximations to real-world data, they satisfy the theoretical conditions in Theorem 2.2.1, 2.3.1, and 2.3.2, including the following additional assumptions that ensure they are, to some extent, biologically meaningful.

- The mortality rate μ (unrelated to disease) assumes an average human lifespan of approximately 76 years, where $\mu = \frac{1}{76 \times 365}$ per day. This is supported by Wise

[36], who predicts global life expectancy will rise from 73.6 years in 2022 to 78.2 years by 2050. Assuming a total population of one million at time ‘t’, the recruitment rate Λ is determined as the product of the total population and μ .

- The proportion θ_i of individuals developing symptoms immediately upon infection from strain- i is based on the study by Massard et al. [22], which provides estimates for various COVID-19 strains. Therefore, $\theta_1 = 0.850$ and $\theta_2 = 0.76$ were chosen as the proportion for strain 1 and 2, respectively.
- The study by Gao et al. [16] estimated identical recovery rates for symptomatic and asymptomatic infections (i.e. $\gamma_{Ii} = \gamma_{Ai}$ for $i = 1, 2$.) for Omicron and Delta at 0.091 per day (≈ 11 days recovery period) and 0.094 per day (≈ 10.6 days recovery period), respectively. However, for the study conducted in this chapter, we assume that symptomatic infections recover more slowly compared to asymptomatic infections. Byrne et al. [4] estimated recovery periods of 6.5-9.5 days for asymptomatic infections and 13.4-18.1 days for symptomatic infections. Hence, the recovery period assumed for strain 1 symptomatic infections is 18 days ($\gamma_{I1} = 0.056$ per day) and 12 days for asymptomatic infections ($\gamma_{A1} = 0.083$ per day). Similarly, for strain 2 symptomatic infections, the recovery period is assumed to be 15 days ($\gamma_{I2} = 0.067$ per day), and 7 days for asymptomatic infections ($\gamma_{A2} = 0.143$ per day).
- The disease-induced mortality rate δ_{Ii} is assumed to exceed δ_{Ai} , reflecting the greater severity associated with symptomatic infections. Based on Massard et al. [22], symptomatic infections typically face disease-induced mortality within 10-14 days of infection onset. Moreover, Huemer et al. [19] reported significantly lower mortality for asymptomatic cases compared to symptomatic ones over a similar observation period. Therefore, it is assumed that strain 1 symptomatic infections suffer disease-induced death after a period of 10 days

($\delta_{I1} = 0.100$ per day) and asymptomatic infections will face disease-induced death after 20 days ($\delta_{A1} = 0.050$ per day). For the case of strain 2 symptomatic infections, it is assumed disease-induced mortality will occur after 14 days ($\delta_{I2} = 0.071$ per day) and asymptomatic infections will face the same fate after 28 days ($\delta_{A2} = 0.071$ per day).

- The proportion κ_{Ai} of asymptomatic individuals transitioning to symptomatic infections are based on values from the two-strain model by Gao et al. [16], which reports daily transition proportions of approximately 40% for the more infectious strain and 20% for the less infectious strain. Accordingly, we assume $\kappa_{A1} = 0.400$ per day and $\kappa_{A2} = 0.200$ per day.
- The waning immunity rate η_{Ai} is assumed to be greater than η_{Ii} , as individuals in compartment R_{Ii} develop stronger immunity after contracting a higher viral dose. A review done by Boyton and Altmann [2] states that asymptomatic infections generate much lower immune responses as opposed to symptomatic infections. A study by Choe [9] states that asymptomatic infections have an approximate waning period of naturally acquired immunity that could range from 5 to 8 months. Another study by Giorgi et al. [13] states that for symptomatic infections, it takes 11 months or more for naturally acquired immunity to wane. Similar studies conducted by Chemaitelly [7] and Goldberg [17] for the context of multiple strains suggest differences in the waning immunity period that span as much as 14 months. Based on these findings, we assume for strain 1 recovered individuals who were symptomatic infections to completely lose their naturally acquired immunity after approximately 14 months ($\eta_{I1} = 0.002$ per day) and 8 months for recovered individuals who were previously strain 1 asymptomatic infections ($\eta_{A1} = 0.004$ per day). Conversely, a waning immunity period of 12 months is assumed for recovered individuals who were strain 2 symptomatic infections ($\eta_{I2} = 0.003$ per day) and 6 months for recovered

individuals who were strain 2 asymptomatic infections ($\eta_{A2} = 0.006$ per day).

- The transmission rate β_{Ii} is assumed to be greater than β_{Ai} because it is assumed that symptomatic infections are more infectious. Therefore, we define $\beta_{Ai} = (1 - C)\beta_{Ii}$, where the constant $0 \leq C \leq 1$ represents the overall reduction in transmission rate for asymptomatic individuals. The study by Gao et al. [16] states that Omicron has an asymptomatic transmission rate that is 30% lower than symptomatic transmission. On the other hand, for Delta it was 25% lower. Other supporting studies, such as that by Tan et al. [33] that had investigated the differences in transmission rate for symptomatic and asymptomatic infections, recorded roughly the same values ($\approx 33.3\%$). Thus, we assume a 30% reduction of transmission probability for asymptomatic infections for either strain ($C = 0.300$).

The parameters listed in Table 2.1 are fixed across all simulations related to the three equilibria cases from Theorem 2.2.1. The only parameters adjusted between cases are the transmission rates β_{Ii} and β_{Ai} , where we select values for $\mathcal{R}_{0,i}$ and solve for the corresponding transmission rates that achieve the desired $\mathcal{R}_{0,i}$ values. Specifically, β_{Ii} is computed based on $\mathcal{R}_{0,i}$, and β_{Ai} is then determined using the reduction factor C ; thus,

$$\beta_{Ii} = \left(\frac{\mathcal{R}_{0,i}}{\Xi_i} \right) \frac{\mu}{\Lambda}, \quad \beta_{Ai} = (1 - C)\beta_{Ii},$$

for $i \in \{1, 2\}$ and

$$\Xi_i = \frac{\theta_i \xi_{Ai} + (1 - \theta_i) \kappa_{Ai}}{\xi_{Ii} \xi_{Ai}} + \frac{(1 - \theta_i)(1 - C)}{\xi_{Ai}}.$$

For the disease-free equilibrium E_0 , both strains must have basic reproduction numbers less than one for local asymptotic stability; therefore, we pick $\mathcal{R}_{0,1} = 0.6$

and $\mathcal{R}_{0,2} = 0.4$. Under these conditions, the computed transmission rates are $\beta_{I1} = 9.484 \times 10^{-8}$, $\beta_{A1} = 4.742 \times 10^{-8}$, $\beta_{I2} = 5.934 \times 10^{-8}$, and $\beta_{A2} = 2.969 \times 10^{-8}$ (units: per person per day).

For the strain-dominant equilibrium \hat{E}_1 to be LAS we must have $R_{0,1} > 1$ and $R_{0,1} > R_{0,2}$; thus, two scenarios are considered. In the first scenario, strain 2 has $R_{0,2} < 1$ and for the second scenario $R_{0,2} > 1$. For the both scenarios we pick $\mathcal{R}_{0,1} = 4$; however, for scenario one we consider $\mathcal{R}_{0,2} = 0.5$ and for the second scenario we pick $\mathcal{R}_{0,2} = 2$. The corresponding transmission rates required to achieve scenario one are $\beta_{I1} = 6.323 \times 10^{-7}$, $\beta_{A1} = 3.161 \times 10^{-7}$, $\beta_{I2} = 7.422 \times 10^{-8}$, and $\beta_{A2} = 3.711 \times 10^{-8}$ (units: per person per day). Furthermore, for scenario two the transmission rates for strain 1 stay the same while strain 2 transmission rates are evaluated as $\beta_{I2} = 2.969 \times 10^{-7}$ and $\beta_{A2} = 1.484 \times 10^{-7}$ (units: per person per day).

Finally, the coexistence equilibria E^* (for $j = 1, 2$), where strains 1 and 2 coexist require equal reproduction numbers; hence, we pick $\mathcal{R}_{0,1} = \mathcal{R}_{0,2} = 2$. The transmission rates are then computed as $\beta_{I1} = 3.161 \times 10^{-7}$, $\beta_{A1} = 1.581 \times 10^{-7}$, $\beta_{I2} = 2.969 \times 10^{-7}$, and $\beta_{A2} = 1.484 \times 10^{-7}$ (units: per person per day).

Having established the parameter values, we now perform numerical simulations to examine the behaviour of symptomatic infections in system (2.1.3) within a local neighbourhood of each equilibrium, providing insights into the stability and dynamics of the solutions under small perturbations.

Figures 2.3 and 2.4 illustrates the evolution of solutions to system (2.1.3) starting from multiple initial conditions and converging toward the strain-1-dominant equilibrium \hat{E}_1 under two distinct scenarios based on the value of $\mathcal{R}_{0,2}$. In Figure 2.3, where $\mathcal{R}_{0,1} > \mathcal{R}_{0,2}$ and $\mathcal{R}_{0,2} < 1$, strain-2 fails to establish itself and rapidly declines, while strain 1 converges directly to its endemic equilibrium. In contrast, Figure 2.4 demonstrates the impact of increasing $\mathcal{R}_{0,2}$ above unity. Provided strain 1 ultimately

Table 2.1: Fixed parameter values used for simulations in the two-strain SIARS model. All values remain constant across all equilibria simulations illustrated in Figures 2.3, 2.4 and 2.5.

Parameter	Value	Unit	Reference
Λ	36.049	Person/Day	Based on a total population of 10^6 and μ .
μ	3.605×10^{-5}	1/Day	Based on [36].
C	0.300	Dimensionless	Based on [16, 33].
θ_1	0.850	Dimensionless	Based on [22].
κ_{A1}	0.400	1/Day	Based on [16]
γ_{I1}	0.056	1/Day	Based on [16, 4].
γ_{A1}	0.083	1/Day	Based on [16, 4].
δ_{I1}	0.100	1/Day	Based on [22, 19].
δ_{A1}	0.050	1/Day	Based on [22, 19].
η_{I1}	0.002	1/Day	Based on [2, 9, 13, 17, 7].
η_{A1}	0.004	1/Day	Based on [2, 9, 13, 17, 7].
θ_2	0.760	Dimensionless	Based on [22].
κ_{A2}	0.200	1/Day	Based from [16]
γ_{I2}	0.067	1/Day	Based on [16, 4].
γ_{A2}	0.143	1/Day	Based on [16, 4].
δ_{I2}	0.071	1/Day	Based on [22, 19].
δ_{A2}	0.036	1/Day	Based on [22, 19].
η_{I2}	0.003	1/Day	Based on [2, 9, 13, 17, 7].
η_{A2}	0.006	1/Day	Based on [2, 9, 13, 17, 7].

dominates, strain 2 initially grows and sustains itself for a prolonged period due to its higher basic reproduction number. This transient behaviour delays the competitive exclusion of strain 2 before eventual decline.

For the case of strain-coexistence equilibria, Figure 2.5 illustrates multiple initial conditions perturbed within 20% of the infinite coexistence equilibrium line. Each initial condition converges to a single equilibrium point on the line, which implies that each equilibrium on the line exhibit neutrally stable behaviour.

The analysis of the strain-dominant equilibrium \hat{E}_1 and the coexistence equilibria E^* provides valuable insights into how differences in transmission rates and the basic reproduction numbers $\mathcal{R}_{0,i}$ drive strain dominance or coexistence in multi-strain

epidemics. The role of waning immunity is also significant, as it influences long-term persistence and the potential for strain coexistence.

Finally, Figure 2.6 provides a clear visualization of how each type of equilibrium is positioned in $\mathcal{R}_{0,i}$ -space, reinforcing the connection between basic reproduction numbers and local stability of equilibria.

Since no health interventions are considered in model (2.1.3), no insights are offered concerning control strategies or preventive measures. Instead, it provides a baseline understanding of the natural competitive dynamics between strains in the absence of intervention. To address this limitation, Chapter 3 extends the model (2.1.3) by incorporating health interventions aimed at reducing new infections and altering epidemic behaviours.

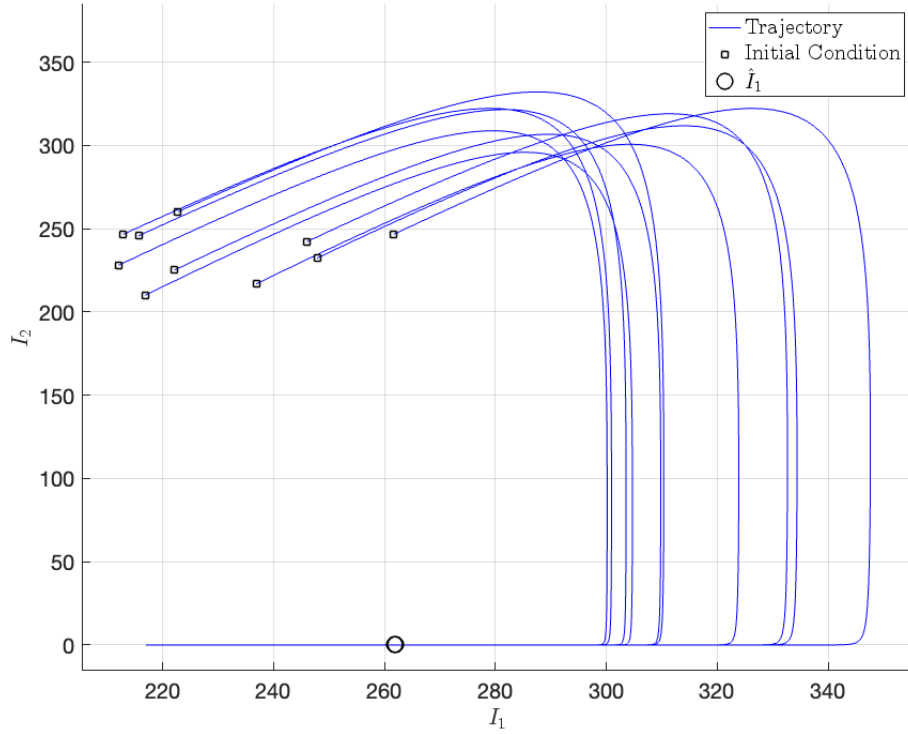


Figure 2.3: Phase portrait illustrating the local dynamics around the strain 1 dominant equilibrium \hat{E}_1 for the case $\mathcal{R}_{0,1} > \mathcal{R}_{0,2}$ with $\mathcal{R}_{0,2} < 1$. Each blue trajectory represents a solution starting from perturbed initial conditions (black squares) in the neighbourhood of the equilibrium. The circle denotes the \hat{I}_1 equilibrium value. All trajectories converge to \hat{E}_1 , demonstrating local asymptotic stability and extinction of strain 2 over time.

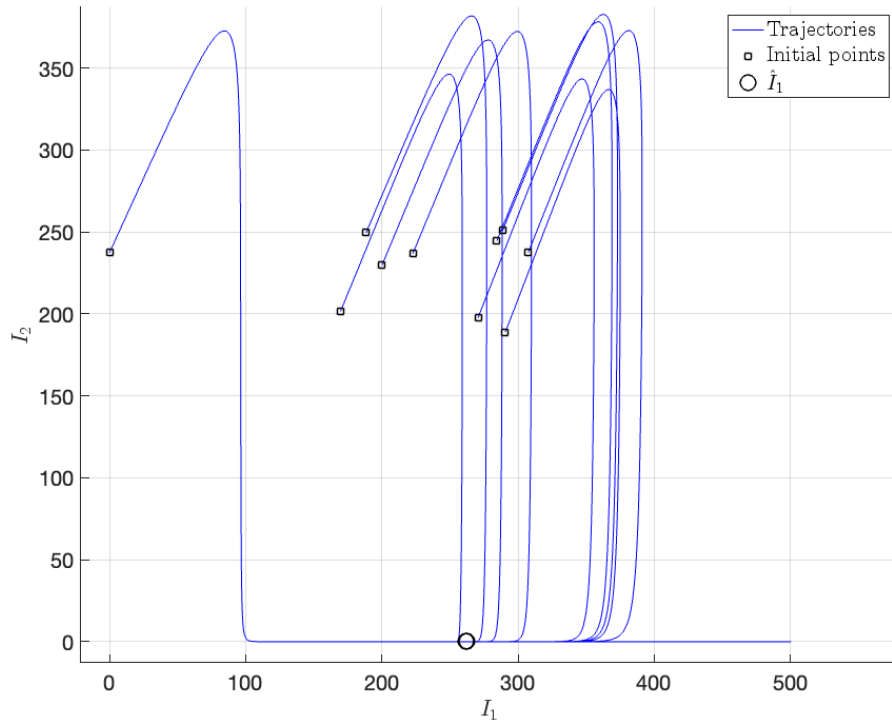


Figure 2.4: Phase portrait illustrating the dynamics near the strain-1-dominant equilibrium \hat{E}_1 for the case $\mathcal{R}_{0,1} > \mathcal{R}_{0,2}$ with $\mathcal{R}_{0,2} > 1$. Among the trajectories, one initial condition is placed exactly at the strain 2 dominant equilibrium coordinate \hat{I}_2 ($I_1(0) = 0$ and $I_2(0) = \hat{I}_2$), which is unstable. Despite $\mathcal{R}_{0,2} > 1$, all trajectories—including the one starting from \hat{I}_2 —eventually converge to the strain-1 equilibrium \hat{I}_1 (marked by the circle), confirming the local asymptotic stability of \hat{E}_1 and extinction of strain 2 over time.

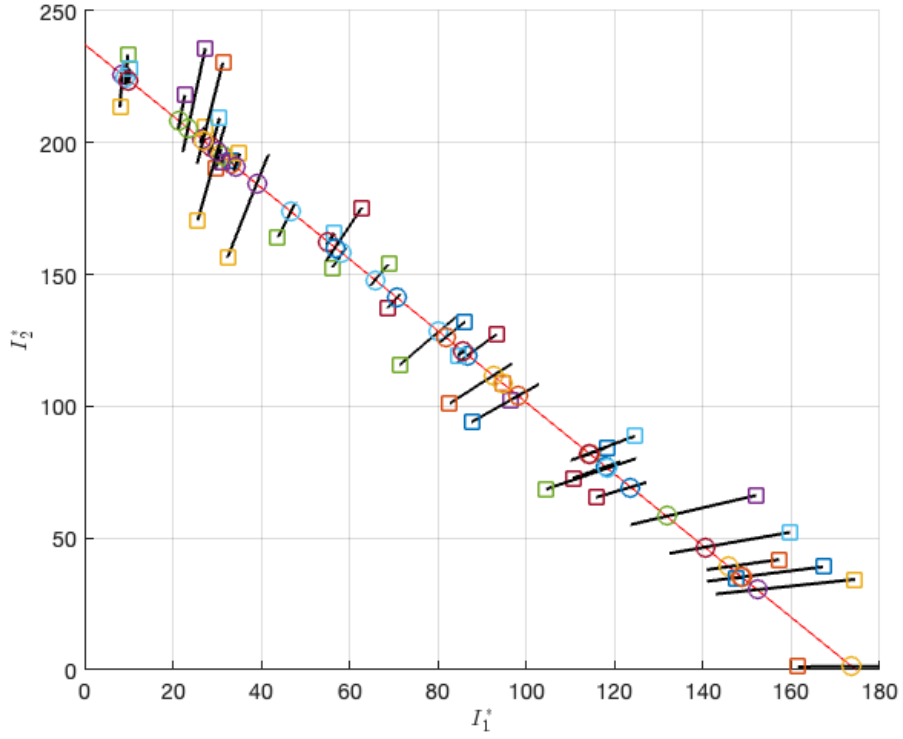


Figure 2.5: Simulation of symptomatic infections in the neighbourhood of the infinite strain-coexistence equilibria E^* for two strains. The figure shows the infinite equilibrium line (solid red line) and solution trajectories (solid black lines) for 40 different initial conditions, each starting at the box marker and ending at the circle marker. Initial conditions were perturbed within 20% of points on the infinite equilibrium line. The coexistence condition $\mathcal{R}_{0,1} = \mathcal{R}_{0,2} > 1$ ensures the existence of the equilibrium line. The results illustrate neutrally stable behaviour, with solutions remaining in the local neighbourhood of the infinite equilibrium line and each initial condition converging to one equilibrium point on the equilibria line.

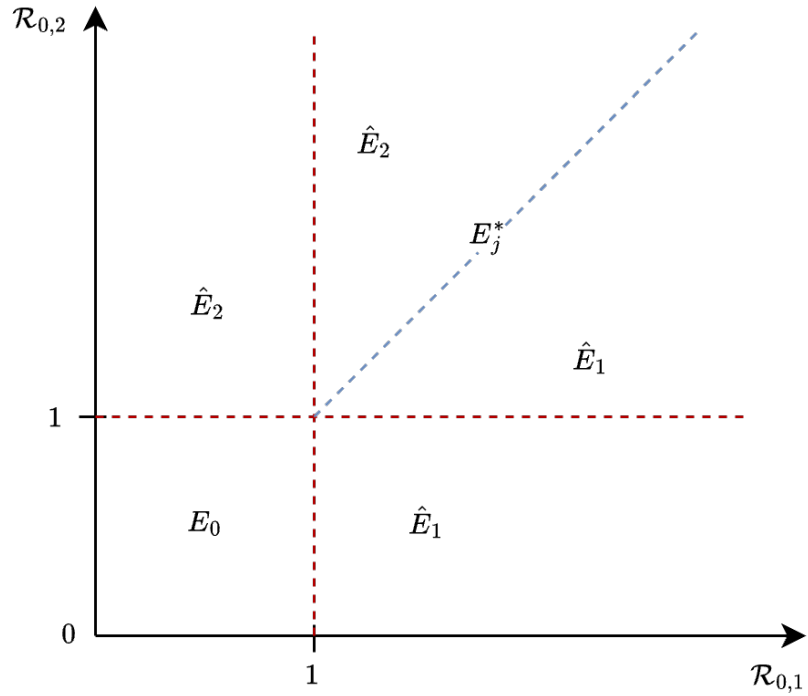


Figure 2.6: Equilibrium stability regions in $\mathcal{R}_{0,i}$ -space for the two-strain SIARS model. The figure illustrates the parameter regions where the disease-free equilibrium E_0 and strain-dominant equilibria \hat{E}_1 and \hat{E}_2 are locally asymptotically stable (LAS). When $\mathcal{R}_{0,1} = \mathcal{R}_{0,2} > 1$, the linearized system stability is inconclusive due to the existence of infinitely many strain-coexistence equilibria E_j^* for $j = 1, 2$. This coexistence region is shown along the diagonal line where both strains can persist.

Chapter 3

A Multi-strain SVIARS model with masking

The model (2.1.3) presented in Chapter 2 is further extended to include two external health interventions; one being masks which are non-pharmaceutical and the other being vaccines which are pharmaceutical.

3.1 Model formulation

In this chapter, we maintain the compartmental classifications defined in system (2.1.3); however, each compartment is now denoted with an additional subscript k , where $k = 1, 2$, and it references the group to which the individuals belong. The two groups portray the distinction between unmasked ($k = 1$) and masked ($k = 2$) individuals within each compartment. Furthermore, we introduce a compartment V_k that accounts for vaccinated-susceptible individuals belonging to group- k .

At any given time ‘ t ’ for group- k , the total population interacting with strains $i = 1, 2, \dots, n$ of an infectious disease, consists of unvaccinated-susceptible individ-

uals $S_k(t)$, vaccinated-susceptible individuals $V_k(t)$, strain- i symptomatic infections $I_{i,k}(t)$, strain- i asymptomatic infections $A_{i,k}(t)$, recovered individuals who transitioned from strain- i symptomatic infections $R_{I_{i,k}}(t)$, and recovered individuals who transitioned from strain- i asymptomatic infections $R_{A_{i,k}}(t)$. Therefore, the total population at time ‘ t ’ is given by

$$N(t) = \sum_{k=1}^2 \left(S_k(t) + V_k(t) + \sum_{i=1}^n (I_{i,k}(t) + A_{i,k}(t) + R_{I_{i,k}}(t) + R_{A_{i,k}}(t)) \right). \quad (3.1.1)$$

Similar to system (2.1.3), we incorporate vital dynamics through the recruitment term Λ_k (units: persons/day), representing the daily influx of fully susceptible individuals into the unvaccinated-susceptible subpopulation. The natural mortality rate μ (unit: 1/day) is assumed to be the same for all groups and its subpopulations regardless of mask-wearing compliance and vaccination.

Unvaccinated-susceptible individuals get vaccinated at a rate ψ_k (unit: 1/day), and it is assumed the vaccine administered to unvaccinated-susceptible individuals will have an efficacy σ , where $0 \leq \sigma \leq 1$. Once vaccinated-susceptible individuals become infected with a given strain- i , it is assumed that all memory/effects of the vaccine are lost.

Inspired from the study by Gumel et.al [18], we incorporate the distinction of inward efficacy ϵ_{in} and outward efficacy ϵ_{out} of masks where, $0 \leq \epsilon_{in} \leq 1$ and $0 \leq \epsilon_{out} \leq 1$. Inward efficacy of masks provides a measure of how well a mask can prevent viral particles from entering the breathing space of a masked individual. On the other hand, outward efficacy provides a measure of how well a mask can prevent viral particles from escaping the mask barrier.

The mask-wearing compliance of individuals in each subpopulation in (3.1.1) are modelled by a parameter ω_{kj} (unit: 1/day) where $j = 1, 2$ and $k \neq j$. The rate at which unmasked individuals start wearing masks is denoted by ω_{12} . Conversely, the

rate at which masked individuals revoke mask-wearing behaviour is represented by ω_{21} .

Unvaccinated and vaccinated susceptible individuals in group- k become infected with a given strain- i by coming in contact with group- k strain- i symptomatic or asymptomatic infections. Transmission occurs at rates $\beta_{Ii,k}$ and $\beta_{Ai,k}$ (unit: $1/(\text{person} \cdot \text{day})$), which represent the per capita risk of transmission. The infection rate, referred to as the force of infection, is denoted by $\vartheta_{i,k}$ and defined as follows:

$$\begin{aligned}\vartheta_{i,1} &= (\beta_{Ii,1}I_{i,1} + \beta_{Ai,1}A_{i,1}) + (1 - \epsilon_{out})(\beta_{Ii,2}I_{i,2} + \beta_{Ai,2}A_{i,2}), \\ \vartheta_{i,2} &= (1 - \epsilon_{in})\vartheta_{i,1}, \\ i &= 1, 2, \dots, n.\end{aligned}\tag{3.1.2}$$

Furthermore, $\vartheta_{i,2}$ implies that as inward mask efficacy increases, the force of infection of masked individuals will decrease. In other words, the functional form of $\vartheta_{i,2}$ implies that the spread of the disease could be controlled by manipulating the inward efficacy of masks. Furthermore, σ acts as a control parameter such that the factor $(1 - \sigma)$ is a constant multiple of each expression in (3.1.2); thus, reducing the probability of vaccinated-susceptible individuals from getting infected.

Upon infection, a proportion $\theta_{i,k}$ (where $0 \leq \theta_{i,k} \leq 1$) of the sum of unvaccinated and vaccinated susceptible individuals immediately develop symptoms and transition into group- k strain- i symptomatic infections. The remaining proportion $(1 - \theta_{i,k})$ become group- k strain- i asymptomatic infections. A fraction of group- k strain- i asymptomatic infections develop symptoms at a rate $\kappa_{Ai,k}$ (unit: $1/\text{day}$) and convert to group- k strain- i symptomatic infections.

Group- k strain- i symptomatic infections recover at rate $\gamma_{Ii,k}$ and asymptomatic infections recover at rate $\gamma_{Ai,k}$ (unit: $1/\text{day}$). Moreover, the disease-induced mortality rates are $\delta_{Ii,k}$ and $\delta_{Ai,k}$ (unit: $1/\text{day}$) respectively. As a result of the recovery rates,

group- k strain- i infected individuals move into the two recovered compartments $R_{Ii,k}$ and $R_{Ai,k}$. Subsequently, the overall naturally acquired immunity wanes at rates $\eta_{Ii,k}$ and $\eta_{Ai,k}$ (unit: 1/day), causing group- k recovered individuals to transition back to group- k unvaccinated-susceptible population. For further simplicity, it is assumed that upon loss of immunity, recovered individuals have an equal probability of becoming infected or reinfected by any strain- i .

Remark. For convenience, we consider the same formalisms in model (2.1.3) for the average time spent in infected and recovered compartments with the additional subscript k referring to the group; thus, we have $\xi_{Ii,k}$, $\xi_{Ai,k}$, $\xi_{RIi,k}$ and $\xi_{RAi,k}$.

The formalism that describes the rate of change of each subpopulation defined in (3.1.1) with respect to time is shown in model (3.1.3), where

$$\begin{aligned}
\frac{dS_k}{dt} &= \Lambda_k - \left(\sum_{i=1}^n \vartheta_{i,k} + \psi_k + \mu \right) S_k + \sum_{i=1}^n (\eta_{Ii,k} R_{Ii,k} + \eta_{Ai,k} R_{Ai,k}) \\
&\quad + \sum_{j \neq k} (\omega_{jk} S_j - \omega_{kj} S_k), \\
\frac{dV_k}{dt} &= \psi_k S_k - \left((1 - \sigma) \sum_{i=1}^n \vartheta_{i,k} + \mu \right) V_k + \sum_{j \neq k} (\omega_{jk} V_j - \omega_{kj} V_k), \\
\frac{dI_{i,k}}{dt} &= \theta_{i,k} \vartheta_{i,k} \left(S_k + (1 - \sigma) V_k \right) + \kappa_{Ai,k} A_{i,k} - \xi_{Ii,k} I_{i,k} \\
&\quad + \sum_{j \neq k} (\omega_{jk} I_{i,j} - \omega_{kj} I_{i,k}), \\
\frac{dA_{i,k}}{dt} &= (1 - \theta_{i,k}) \vartheta_{i,k} \left(S_k + (1 - \sigma) V_k \right) - \xi_{Ai,k} A_{i,k} \\
&\quad + \sum_{j \neq k} (\omega_{jk} A_{i,j} - \omega_{kj} A_{i,k}), \\
\frac{dR_{Ii,k}}{dt} &= \gamma_{Ii,k} I_{i,k} - \xi_{RIi,k} R_{Ii,k} + \sum_{j \neq k} (\omega_{jk} R_{Ii,j} - \omega_{kj} R_{Ii,k}), \\
\frac{dR_{Ai,k}}{dt} &= \gamma_{Ai,k} A_{i,k} - \xi_{RAi,k} R_{Ai,k} + \sum_{j \neq k} (\omega_{jk} R_{Ai,j} - \omega_{kj} R_{Ai,k}),
\end{aligned} \tag{3.1.3}$$

$i = 1, 2, \dots, n$ and $j, k = 1, 2$ with $j \neq k$.

The system (3.1.3) admits a solution of the form $(S_1, V_1, \mathbf{SV}_{1,1}, \mathbf{SV}_{2,1}, \dots, \mathbf{SV}_{n,1}, S_2, V_2, \mathbf{SV}_{1,2}, \mathbf{SV}_{2,2}, \dots, \mathbf{SV}_{n,2}) \in \mathbb{R}_+^{8n+4}$, where $\mathbf{SV}_{i,k} = [I_{i,k}, A_{i,k}, R_{I_{i,k}}, R_{A_{i,k}}]$ is a vector that contains the infected and recovered compartments corresponding to strain $i \in \{1, 2, \dots, n\}$ and group $k \in \{1, 2\}$. The diagram that illustrates system (3.1.3) is shown in Figure 3.1. The following theorem shows that model (3.1.3) admits unique, globally defined, and non-negative solutions.

Theorem 3.1.1. *For any given initial condition $(S_1(0), V_1(0), \mathbf{SV}_{1,1}(0), \mathbf{SV}_{2,1}(0), \dots, \mathbf{SV}_{n,1}(0), S_2(0), V_2(0), \mathbf{SV}_{1,2}(0), \mathbf{SV}_{2,2}(0), \dots, \mathbf{SV}_{n,2}(0)) \in \mathbb{R}_+^{8n+4}$, there exists a unique solution to model (3.1.3) which exists globally, remains non-negative and is bounded.*

Proof. Note that the functions on the right-hand side of model (3.1.3) are continuously differentiable. It follows from the Fundamental Existence-Uniqueness Theorem [29] that model (3.1.3) admits a unique solution on $[0, \tau)$ for some $\tau > 0$

The approach to show the non-negativity of solutions for model (3.1.3) follows analogously to that of model (2.1.3) as elaborated in the proof for Theorem 2.1.1. By applying the same invariant region arguments and boundary analyses, it can be shown that all state variables of (3.1.3) remain non-negative for all $t \geq 0$. Details are omitted for brevity.

Next, we show the solution $(S_1, V_1, \mathbf{SV}_{1,1}, \mathbf{SV}_{2,1}, \dots, \mathbf{SV}_{n,1}, S_2, V_2, \mathbf{SV}_{1,2}, \mathbf{SV}_{2,2}, \dots, \mathbf{SV}_{n,2}) \in \mathbb{R}_+^{8n+4}$ is bounded. Note that

$$\frac{dN}{dt} = \Lambda_1 + \Lambda_2 - \mu N - \sum_{k=1}^2 \sum_{i=1}^n (\delta_{I_{i,k}} I_{i,k} + \delta_{A_{i,k}} A_{i,k}).$$

It follows from the non-negativity of the solution that

$$\frac{dN}{dt} \leq \Lambda_1 + \Lambda_2 - \mu N,$$

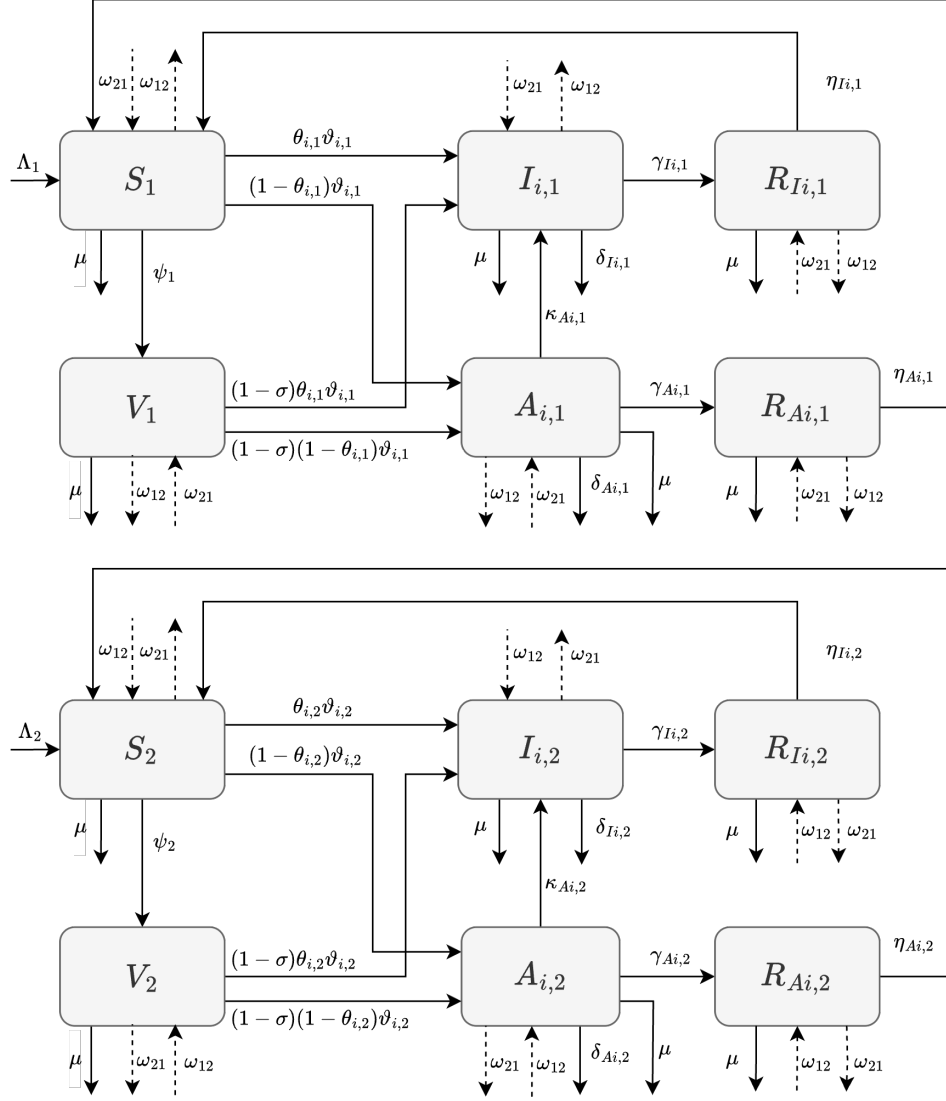


Figure 3.1: A multi-strain SVIARS model with masking. Considering $k \in \{1, 2\}$ and $i \in \{1, 2, \dots, n\}$, new individuals enter the group- k unvaccinated-susceptible compartment S_k at rate Λ_k and receive vaccination at rate ψ_k which causes the transition to V_k . A fraction $\theta_{i,k}$ of group- k strain- i susceptible individuals transition to symptomatic infections ($I_{i,k}$) and the remaining portion $(1 - \theta_{i,k})$ transitions to asymptomatic infections ($A_{i,k}$) at rate $\vartheta_{i,k}$. Group- k strain- i asymptomatic infections develop symptoms at rate $\kappa_{A_{i,k}}$. Recovery for symptomatic and asymptomatic infections occurs at rates $\gamma_{I_{i,k}}$ and $\gamma_{A_{i,k}}$, leading to respective recovered compartments ($R_{I_{i,k}}$ and $R_{A_{i,k}}$). Immunity wanes at rates $\eta_{I_{i,k}}$ and $\eta_{A_{i,k}}$, returning individuals to the compartment S_k . All compartments have natural mortality rate μ except for disease-induced mortality $\delta_{I_{i,k}}$ and $\delta_{A_{i,k}}$ that are exclusive for group- k strain- i symptomatic and asymptomatic infections.

which yields

$$N(t) \leq \frac{\Lambda_1 + \Lambda_2}{\mu} + \left(N(0) - \frac{\Lambda_1 + \Lambda_2}{\mu} \right) e^{-\mu t}.$$

Thus,

$$N(t) \leq \max \left(N(0), \frac{\Lambda_1 + \Lambda_2}{\mu} \right),$$

and

$$\limsup_{t \rightarrow \infty} N(t) \leq \frac{\Lambda_1 + \Lambda_2}{\mu}.$$

Therefore, the solution is bounded and hence exists globally. \square

3.2 The disease-free equilibrium and basic reproduction number

In contrast to equilibria investigations conducted in Chapter 2, for model (3.1.3) we focus specifically on the disease-free equilibrium (DFE), which is followed by the evaluation of the basic reproduction number \mathcal{R}_0 due to its insights about which factors can aid in the prevention of a disease outbreak. The DFE only consists of unvaccinated-susceptible and vaccinated-susceptible individuals who remain fully susceptible until a viral agent is introduced into the population. Due to the increased complexity introduced by masking, vaccination, and movement between groups in model (3.1.3), endemic equilibria will not be examined.

Theorem 3.2.1. *In system (3.1.3), there exists exactly one unique DFE denoted by:*

$$\mathbb{E}_0 = (S_{1,0}, V_{1,0}, \mathbf{SV}_{1,1}, \mathbf{SV}_{2,1}, \dots, \mathbf{SV}_{n,1}, S_{2,0}, V_{2,0}, \mathbf{SV}_{1,2}, \mathbf{SV}_{2,2}, \dots, \mathbf{SV}_{n,2}) \in \mathbb{R}_+^{8n+2},$$

where

$$S_{1,0} = \frac{\omega_{21}\Lambda_2 + (\psi_2 + \omega_{21} + \mu)\Lambda_1}{(\psi_2 + \mu)(\psi_1 + \omega_{12} + \mu) + \omega_{21}(\psi_1 + \mu)}, \quad V_{1,0} = \frac{(\omega_{21} + \mu)\psi_1 S_{1,0} + \omega_{21}\psi_2 S_{2,0}}{\mu(\omega_{12} + \omega_{21} + \mu)},$$

$$S_{2,0} = \frac{\omega_{12}\Lambda_1 + (\psi_1 + \omega_{12} + \mu)\Lambda_2}{(\psi_2 + \mu)(\psi_1 + \omega_{12} + \mu) + \omega_{21}(\psi_1 + \mu)}, \quad V_{2,0} = \frac{\psi_1\omega_{12}S_{1,0} + \psi_2(\omega_{12} + \mu)S_{2,0}}{\mu(\omega_{12} + \omega_{21} + \mu)},$$

and

$$\mathbf{S}\mathbf{V}_{i,1} = \mathbf{S}\mathbf{V}_{i,2} = \mathbf{0}_{4 \times 1} \text{ for } i = 1, 2, \dots, n.$$

Proof. We begin by assuming that the DFE for system (3.1.3) has no recovered individuals present. When the derivatives on the left hand side of system (3.1.3) is equated to zero and evaluated at the DFE it yields the two linear systems,

$$\begin{aligned} 0 &= \Lambda_1 - (\psi_1 + \omega_{12} + \mu)S_{1,0} + \omega_{21}S_{2,0} \\ 0 &= \Lambda_2 - (\psi_2 + \omega_{21} + \mu)S_{2,0} + \omega_{12}S_{1,0} \end{aligned} \tag{3.2.1}$$

and

$$\begin{aligned} 0 &= \psi_1 S_{1,0} - (\omega_{12} + \mu)V_{1,0} + \omega_{21}V_{2,0} \\ 0 &= \psi_2 S_{2,0} - (\omega_{21} + \mu)V_{2,0} + \omega_{12}V_{1,0} \end{aligned} \tag{3.2.2}$$

Solving the linear system (3.2.1) gives the two solutions $S_{1,0}$ and $S_{2,0}$ as stated in the theorem. Similarly, $S_{1,0}$ and $S_{2,0}$ are substituted into the linear system (3.2.2) and solved to obtain the solutions stated in the theorem for $V_{1,0}$ and $V_{2,0}$. \square

Following the approach in Chapter 2, the basic reproduction number \mathcal{R}_0 for system (3.1.3) is derived using the next-generation matrix method by van den Driessche and Watmough [35]. The system is reformulated as $\dot{Y} = \mathcal{F} - \mathcal{V}$, where $Y = [I_{1,1} \ I_{1,2} \ A_{1,1} \ A_{1,2} \ \dots \ I_{n,1} \ I_{n,2} \ A_{n,1} \ A_{n,2}]$ is the vector of infected compartments. The

vector of new infections \mathcal{F} is given as

$$\mathcal{F} = \begin{pmatrix} \theta_{1,1}\vartheta_{1,1} [S_1 + (1 - \sigma)V_1] \\ \theta_{1,2}\vartheta_{1,2} [S_2 + (1 - \sigma)V_2] \\ (1 - \theta_{1,1})\vartheta_{1,1} [S_1 + (1 - \sigma)V_1] \\ (1 - \theta_{1,2})\vartheta_{1,2} [S_2 + (1 - \sigma)V_2] \\ \vdots \\ \theta_{n,1}\vartheta_{n,1} [S_1 + (1 - \sigma)V_1] \\ \theta_{n,2}\vartheta_{n,2} [S_2 + (1 - \sigma)V_2] \\ (1 - \theta_{n,1})\vartheta_{n,1} [S_1 + (1 - \sigma)V_1] \\ (1 - \theta_{n,2})\vartheta_{n,2} [S_2 + (1 - \sigma)V_2] \end{pmatrix},$$

and the vector of transitions \mathcal{V} is expressed as

$$\mathcal{V} = \begin{pmatrix} \xi_{I1,1}I_{1,1} - \kappa_{A1,1}A_{1,1} - \omega_{21}I_{1,2} + \omega_{12}I_{1,1} \\ \xi_{I1,2}I_{1,2} - \kappa_{A1,2}A_{1,2} - \omega_{12}I_{1,1} + \omega_{21}I_{1,2} \\ \xi_{A1,1}A_{1,1} - \omega_{21}A_{1,2} + \omega_{12}A_{1,1} \\ \xi_{A1,2}A_{1,2} - \omega_{12}A_{1,1} + \omega_{21}A_{1,2} \\ \vdots \\ \xi_{In,1}I_{n,1} - \kappa_{An,1}A_{n,1} - \omega_{21}I_{n,2} + \omega_{12}I_{n,1} \\ \xi_{In,2}I_{n,2} - \kappa_{An,2}A_{n,2} - \omega_{12}I_{n,1} + \omega_{21}I_{n,2} \\ \xi_{An,1}A_{n,1} - \omega_{21}A_{n,2} + \omega_{12}A_{n,1} \\ \xi_{An,2}A_{n,2} - \omega_{12}A_{n,1} + \omega_{21}A_{n,2} \end{pmatrix}.$$

Using vectors \mathcal{F} and \mathcal{V} , we evaluate the matrix of new infections \mathbf{F} and the matrix of transitions \mathbf{V} , where $\mathbf{F} = \frac{\partial \mathcal{F}}{\partial \mathbf{Y}}$ and $\mathbf{V} = \frac{\partial \mathcal{V}}{\partial \mathbf{Y}}$. At the DFE, the unvaccinated-susceptible population and vaccinated susceptible populations are combined into one parameter

$$\Delta_{k,0} = S_{k,0} + (1 - \sigma)V_{k,0},$$

for $k = 1, 2$ and substituted to the matrix \mathbf{F} which yields,

$$\mathbf{F} = \begin{pmatrix} \mathbf{F}_1 & \dots & 0 \\ \vdots & \ddots & \vdots \\ 0 & \dots & \mathbf{F}_n \end{pmatrix}.$$

The sub-matrices $\mathbf{F}_i \in \mathbb{R}^{4 \times 4}$ correspond to each strain $i = 1, 2, \dots, n$ and is also expressed as an inner product of two vectors, such that

$$\mathbf{F}_i = \mathbf{k}^T \mathbf{f}_i,$$

where

$$\mathbf{f}_i = \begin{pmatrix} \beta_{Ii,1} & (1 - \epsilon_{out})\beta_{Ii,2} & \beta_{Ai,1} & (1 - \epsilon_{out})\beta_{Ai,2} \end{pmatrix},$$

and

$$\mathbf{k} = \begin{pmatrix} \theta_{i,1}\Delta_{1,0} & \theta_{i,2}(1 - \epsilon_{in})\Delta_{2,0} & (1 - \theta_{i,1})\Delta_{1,0} & (1 - \theta_{i,2})(1 - \epsilon_{in})\Delta_{2,0} \end{pmatrix}.$$

The matrix of transitions is

$$\mathbf{V} = \begin{pmatrix} \mathbf{V}_1 & \dots & 0 \\ \vdots & \ddots & \vdots \\ 0 & \dots & \mathbf{V}_n \end{pmatrix},$$

and the sub-matrices \mathbf{V}_i for $i = 1, 2, \dots, n$ are of the form,

$$\mathbf{V}_i = \begin{pmatrix} \omega_{12} + \xi_{Ii,1} & -\omega_{21} & -\kappa_{Ai,1} & 0 \\ -\omega_{21} & \omega_{21} + \xi_{Ii,2} & 0 & -\kappa_{Ai,2} \\ 0 & 0 & \omega_{12} + \xi_{Ai,1} & -\omega_{21} \\ 0 & 0 & -\omega_{12} & \omega_{21} + \xi_{Ai,2} \end{pmatrix}.$$

The next-generation matrix is \mathbf{G} , where $\mathbf{G} = \mathbf{F}\mathbf{V}^{-1}$ is expressed as,

$$\mathbf{G} = \begin{pmatrix} \mathbf{G}_1 & \dots & 0 \\ \vdots & \ddots & \vdots \\ 0 & \dots & \mathbf{G}_n \end{pmatrix}.$$

The sub-matrices $\mathbf{G}_i \forall i = 1, 2, \dots, n$ of the next-gen matrix \mathbf{G} has the form $\mathbf{G}_i \in \mathbb{R}^{4 \times 4}$ and is expressed as an inner product of two vectors, where

$$\mathbf{G}_i = \mathbf{k}^T \Phi_i.$$

The vector \mathbf{k} is the same as that used in sub-matrix \mathbf{F}_i ; however, the vector $\Phi_i = \begin{pmatrix} a_i & b_i & c_i & d_i \end{pmatrix}$, where

$$\begin{aligned} a_i &= \frac{\beta_{Ii,1}(\omega_{21} + \xi_{Ii,2})}{\omega_{21}\xi_{Ii,1} + \xi_{Ii,2}(\omega_{12} + \xi_{Ii,1})} + \frac{(1 - \epsilon_{out})\beta_{Ii,2}\omega_{12}}{\omega_{12}\xi_{Ii,2} + \xi_{Ii,1}(\omega_{21} + \xi_{Ii,2})}, \\ b_i &= \frac{\beta_{Ii,1}\omega_{21}}{\omega_{21}\xi_{Ii,1} + \xi_{Ii,2}(\omega_{12} + \xi_{Ii,1})} + \frac{(1 - \epsilon_{out})\beta_{Ii,2}(\omega_{12} + \xi_{Ii,1})}{\omega_{12}\xi_{Ii,2} + \xi_{Ii,1}(\omega_{21} + \xi_{Ii,2})}, \\ c_i &= \frac{\beta_{Ii,1} \left[\kappa_{Ai,1}(\omega_{21} + \xi_{Ii,2})(\omega_{21} + \xi_{Ai,2}) + \kappa_{Ai,2}\omega_{12}\omega_{21} \right]}{\left[\omega_{21}\xi_{Ii,1} + \xi_{Ii,2}(\omega_{12} + \xi_{Ii,1}) \right] \left[\omega_{21}\xi_{Ai,1} + \xi_{Ai,2}(\omega_{12} + \xi_{Ai,1}) \right]} \\ &\quad + \frac{(1 - \epsilon_{out})\beta_{Ii,2}\omega_{12} \left[\kappa_{Ai,1}(\omega_{21} + \xi_{Ai,2}) + \kappa_{Ai,2}(\omega_{12} + \xi_{Ii,1}) \right]}{\left[\omega_{12}\xi_{Ii,2} + \xi_{Ii,1}(\omega_{21} + \xi_{Ii,2}) \right] \left[\omega_{12}\xi_{Ai,2} + \xi_{Ai,1}(\omega_{21} + \xi_{Ai,2}) \right]} \\ &\quad + \frac{\beta_{Ai,1}(\omega_{21} + \xi_{Ai,2})}{\omega_{21}\xi_{Ai,1} + \xi_{Ai,2}(\omega_{12} + \xi_{Ai,1})} + \frac{(1 - \epsilon_{out})\beta_{Ai,2}\omega_{12}}{\omega_{12}\xi_{Ai,2} + \xi_{Ai,1}(\omega_{21} + \xi_{Ai,2})}, \\ d_i &= \frac{(1 - \epsilon_{out})\beta_{Ii,2} \left[\kappa_{Ai,1}\omega_{12}\omega_{21} + \kappa_{Ai,2}(\omega_{12} + \xi_{Ii,1})(\omega_{12} + \xi_{Ai,1}) \right]}{\left[\omega_{12}\xi_{Ii,2} + \xi_{Ii,1}(\omega_{21} + \xi_{Ii,2}) \right] \left[\omega_{12}\xi_{Ai,2} + \xi_{Ai,1}(\omega_{21} + \xi_{Ai,2}) \right]} \\ &\quad + \frac{\beta_{Ii,1}\omega_{21} \left[\kappa_{Ai,1}(\omega_{21} + \xi_{Ii,2}) + \kappa_{Ai,2}(\omega_{12} + \xi_{Ai,1}) \right]}{\left[\omega_{12}\xi_{Ii,2} + \xi_{Ii,1}(\omega_{21} + \xi_{Ii,2}) \right] \left[\omega_{12}\xi_{Ai,2} + \xi_{Ai,1}(\omega_{21} + \xi_{Ai,2}) \right]} \\ &\quad + \frac{\beta_{Ai,1}\omega_{21}}{\omega_{21}\xi_{Ai,1} + \xi_{Ai,2}(\omega_{12} + \xi_{Ai,1})} + \frac{(1 - \epsilon_{out})\beta_{Ai,2}(\omega_{12} + \xi_{Ai,1})}{\omega_{12}\xi_{Ai,2} + \xi_{Ai,1}(\omega_{21} + \xi_{Ai,2})}, \end{aligned} \tag{3.2.3}$$

$i = 1, 2, \dots, n.$

Moreover, the zeros on the off-diagonals of the next-gen matrix \mathbf{G} form triangular null matrices. It can be noted that the matrices \mathbf{G}_i are all rank 1; therefore, of the four eigenvalues, one is non-zero and the other three are zero. The non-zero eigenvalue $\forall i \in \{1, 2, \dots, n\}$ is the trace of matrix \mathbf{G}_i , where $\lambda_i = \text{tr}(\mathbf{G}_i) = \Phi_i \mathbf{k}^T$. The eigenvalue λ_i consists of parameters exclusive to strain- i ; hence, we represent each non-zero eigenvalue of the next generation matrix \mathbf{G} as the basic reproduction number of each strain, where

$$\begin{aligned} \mathcal{R}_{0,i} &= \left(\theta_{i,1} a_i + (1 - \theta_{i,1}) c_i \right) \Delta_{1,0} + (1 - \epsilon_{in}) \left(\theta_{i,2} b_i + (1 - \theta_{i,2}) d_i \right) \Delta_{2,0}, \\ & i = 1, 2, \dots, n. \end{aligned} \quad (3.2.4)$$

The overall basic reproduction number \mathcal{R}_0 of the entire system (3.1.3) is the spectral radius of matrix \mathbf{G} , where $\mathcal{R}_0 = \rho(\mathbf{G}) = \max\{\mathcal{R}_{0,i}\}$. Therefore, we have the following theorem that describes the local stability of the DFE and is based on the works by Watmough and van den Driessche [35].

Theorem 3.2.2. *When $\mathcal{R}_0 < 1$ the DFE \mathbb{E}_0 is LAS. Conversely, when $\mathcal{R}_0 > 1$, E_0 is unstable.*

Given the analytical complexity of model (3.1.3), in the following section, we focus on numerical analyses to determine health intervention thresholds. To do so, we pick approximations for baseline values based on past studies and vary each health intervention-related parameter and investigate its influence on the solutions to model (3.1.3).

3.3 Numerical simulations and discussions

To conduct numerical analyses, we first establish approximations for baseline parameter values with reference to past literature. Approximations provide a reasonable

basis for analyzing how model parameters influence outcomes of interest. For further simplicity, we assume the values for parameters in model (3.1.3) for both groups are equal to each other (e.g. $\gamma_{Ii,1} = \gamma_{Ii,2}$). Since model (3.1.3) is an extension to model (2.1.3), we recall and use the values in Table 2.1 for the majority of the parameters. The approximations for baseline parameter values that are unique to model (3.1.3) are listed in Table 3.1.

It is assumed that the mask-wearing compliance of every individual will not occur at the same time; therefore, the rates ω_{12} and ω_{21} are based on averaged behaviour. A study done by Adjodah et al. [14] had investigated mask-wearing adherence in various regions of the USA, and within 40 days, there was a 23.4% increase in mask-adherence from a standard range of 40-60%. The percentage increase corresponds to a daily masking compliance rate of 0.006 per day.

Another study done by Nagata et al. [23] in Japan, observed an overall mask abandonment of 28% from 97% to 69% over a much longer period of 265 days. The study assumes exponential decline and the result portrays a mask abandonment rate of 0.001 per day. Similar values were shown in the study by Gumel et al. [18] for the USA, where the mask-adherence rate was found to be 0.006229 (≈ 0.006) per day and the mask abandonment rate was calculated to be 0.000798 (≈ 0.001) per day.

Due to the similarity between the values in studies [14, 18, 23], we consider $\omega_{12} = 0.006$ per day and $\omega_{21} = 0.001$ per day, to be good benchmarks upon which the baseline values are defined for the numerical analyses in this chapter. In light of the results portrayed in the referenced studies, the mask-wearing compliance rate ω_{21} is assumed to be lower than ω_{12} because individuals who wear masks could be less prone to removing them as opposed to those who were not wearing masks initially.

In the study conducted by Gumel et al. [18], the vaccination rate is assumed to be 2.97×10^{-4} per day, and the same value is considered for both unmasked and masked

groups of individuals. In addition, we investigate the findings in another study by Childs et al. [8] that develops a strategy for vaccinating 80% of the population in Canada by aiming for monthly coverages ranging from 1-19% over 8 months. Inspired by the the daily vaccination rate formulation in the study by Childs et al. [8], with the assumption that there would be an overall average of 10% coverage monthly for the population, we form the vaccination rate for unmasked susceptible individuals to be $\psi_1 = 3.333 \times 10^{-3}$ per day. However, the studies done by Gumel et al. [18] and Childs et al. [8] do not consider differences in vaccination rates for masked and unmasked individuals.

A paper by Nguyen et al. [24] states that masked individuals are much more likely to get themselves vaccinated as opposed to those who are unmasked, where the odds of unmasked individuals vaccinating themselves are up to 6 to 12 times lower compared to masked individuals. Based on this observation, we adopt a mid-range estimate and assume that unmasked individuals are nine times less likely to get vaccinated, which implies $\psi_2 = 31.608 \times 10^{-3}$ per day for masked individuals.

In the context of masking efficacies (ϵ_{in} and ϵ_{out}), a study by Pan et al. [28] describes various types of masks such as cloth masks, surgical masks, KN95, etc., and investigate its efficacies for stopping micro-particles of multiple sizes. A similar study was conducted by Duncan et al. [32] for the protective efficacies of KN95 and N95 masks specifically for controlling viral particles associated to SARS-CoV-2. Assuming the mask-wearer has a good fit for the mask that is been worn, a baseline range for inward efficacy ϵ_{in} is thought to be between 20-40%. Furthermore, a baseline range for outward efficacy ϵ_{out} is assumed to be between 35-65%. Based on the referenced studies by Pan et al. [28] and Duncan et al. [32], the stated ranges were formed assuming that all viral-based particle sizes are less than 1 micrometer.

A study by Wu et al. [38] investigated the long-term effects of vaccination against

COVID19. Provided the study had distinguished differences in vaccine strength and its control effects for different strains of the disease, a baseline range of varying levels of efficacy lies between 43-89%. In the paper by Gumel et al. [18], the maximum vaccine efficacy was 95% recorded for Moderna and Pfizer. Therefore, in the simulations conducted in this chapter, we will assume a baseline value for the vaccine efficacy to be $\sigma = 0.7$, which corresponds to a vaccine that is 70% effective in reducing the probability of a vaccinated-susceptible individual contracting a given disease.

Table 3.1: Baseline health-intervention related parameter values used for simulations in the two-strain SVIARS model with masking.

Parameter	Value	Unit	Reference
σ	0.700	Dimensionless	Approximately based on [18, 38].
ϵ_{in}	0.300	Dimensionless	Based on [28, 32].
ϵ_{out}	0.500	Dimensionless	Based on [28, 32].
ψ_1	3.333×10^{-3}	1/Day	Based on [8, 18].
ψ_2	31.608×10^{-3}	1/Day	Based on [24].
ω_{12}	0.006	1/Day	Based on [14, 18].
ω_{21}	0.001	1/Day	Based on [18, 23].

Our first set of simulations focuses on the behaviour of solutions to model (3.1.3) in the context of the disease-free equilibrium \mathbb{E}_0 stated in Theorem 3.2.1, where the overall basic reproduction number \mathcal{R}_0 must be less than unity for local stability. The symptomatic infections for strains 1 and 2 in both masked and unmasked groups, starting from three initial conditions, can be seen diminishing in the phase portraits illustrated in Figure 3.2.

The health-intervention related parameter values used to generate the plots in Figure 3.2 are exactly those seen in Table 3.1 with the exception that vaccine efficacy $\sigma = 0.8$, and hence it yields the strain-specific basic reproduction numbers $\mathcal{R}_{0,1} = 0.724$ and $\mathcal{R}_{0,2} = 0.362$. The overall $\mathcal{R}_0 = \max\{\mathcal{R}_{0,1}, \mathcal{R}_{0,2}\} = 0.724$, which is less than one and corresponds to the DFE being locally stable. Moreover, if we consider the baseline vaccine efficacy (i.e., $\sigma = 0.7$), it results in the strain-specific basic

reproduction numbers to be $\mathcal{R}_{0,1} = 1.429$ and $\mathcal{R}_{0,2} = 0.714$. The overall basic reproduction number $\mathcal{R}_0 = 1.429$ being greater than one implies that the DFE is unstable.

Considering the unstable case for the DFE, the phase portraits shown in Figure 3.3 illustrate strain 2 symptomatic infections in both unmasked and masked groups converging to zero, while the strain 1 symptomatic infections in both groups converge to different non-zero points starting from different initial conditions. The behaviours associated with strain 1 can be closely related to strain-dominant equilibria previously mentioned in Chapter 2. The key difference is that solutions do not approach a unique strain-dominant equilibrium value, instead, every initial condition is attracted by a particular equilibrium value for strain 1 symptomatic infections.

Provided the simulations in Figure 3.2 and Figure 3.3 demonstrate the behaviour of solutions to model (3.1.3) under specific parameter considerations, there is no basis to determine strategies for controlling the spread of a given infectious disease. To address this, we employ a more focused approach in the next section concerning each parameter listed in Table 3.1.

3.4 Focused investigations for health-intervention related parameters

The partial derivative of the strain- i basic reproduction number $\mathcal{R}_{0,i}$ in equation (3.2.4) with respect to parameters σ and ϵ_{in} yields

$$\frac{\partial \mathcal{R}_{0,i}}{\partial \sigma} = -\left(\theta_{i,1}a_i + (1 - \theta_{i,1})c_i\right)V_{1,0} - (1 - \epsilon_{in})\left(\theta_{i,2}b_i + (1 - \theta_{i,2})d_i\right)V_{2,0} < 0,$$

and

$$\frac{\partial \mathcal{R}_{0,i}}{\partial \epsilon_{in}} = -\left(\theta_{i,2}b_i + (1 - \theta_{i,2})d_i\right)\Delta_{2,0} < 0.$$

Furthermore, the partial derivative of the strain- i basic reproduction number $\mathcal{R}_{0,i}$ with respect to ϵ_{out} gives

$$\frac{\partial \mathcal{R}_{0,i}}{\partial \epsilon_{out}} = \left(\theta_{i,1}\frac{\partial a_i}{\partial \epsilon_{out}} + (1 - \theta_{i,1})\frac{\partial c_i}{\partial \epsilon_{out}}\right)\Delta_{1,0} + (1 - \epsilon_{in})\left(\theta_{i,2}\frac{\partial b_i}{\partial \epsilon_{out}} + (1 - \theta_{i,2})\frac{\partial d_i}{\partial \epsilon_{out}}\right)\Delta_{2,0} < 0.$$

The result is negative because the partial derivatives of a_i , b_i , c_i and d_i in equation (3.2.3) when differentiated with respect to ϵ_{out} , are negative.

Provided that the partial derivatives signify linearly decreasing gradients, for further assurance, the illustrations in Figure 3.4 and Figure 3.6 shows the behaviour of the overall basic reproduction number \mathcal{R}_0 for a two-strain scenario with respect to variations in parameters σ , ϵ_{in} and ϵ_{out} accordingly.

In Figure 3.4, it is evident that the relationship between the overall basic reproduction number \mathcal{R}_0 and vaccine efficacy σ is linear. A key feature that can be noted is that \mathcal{R}_0 falls below the threshold $\mathcal{R}_0 = 1$ within vaccine efficacies of 0.7 and 0.8; thus, the behaviours portrayed earlier in Figure 3.2 and Figure 3.3 are further justified. This not only reinforces the importance of vaccine effectiveness in epidemic control but also offers a direct estimate of the minimum efficacy required to achieve local stability for the DFE, assuming all other parameter values in Table 2.1 (identical for both unmasked and masked individuals) and Table 3.1 remain unchanged.

The contour plot shown in Figure 3.6 highlights the influence of inward efficacy ϵ_{in} and outward efficacy ϵ_{out} of masks on the overall basic reproduction number \mathcal{R}_0 . Notably, the contour regions demonstrate a nonlinear, synergistic interaction between the two masking efficacies, and the threshold $\mathcal{R}_0 = 1$ is represented by the white dotted line, beyond which there will be no disease outbreak and system (3.1.3)

will reach the stable steady-state of the DFE. Thus, the results portrayed in Figure 3.4 and Figure 3.6 provide approximate benchmarks that could aid in designing or improving vaccines and masks to the required efficacy levels.

The partial derivatives of $\mathcal{R}_{0,i}$ in equation (3.2.4) with respect to the other parameters related to health interventions, i.e., vaccination rates ψ_1 and ψ_2 and masking compliance rates ω_{12} and ω_{21} , are not trivial. Therefore, the illustrations in Figure 3.5 and Figure 3.7 portray the variations in the overall basic reproduction number \mathcal{R}_0 for a two-strain scenario as each parameter is varied.

To understand the impact of varying vaccination rates (ψ_1 and ψ_2) on the overall basic reproduction number \mathcal{R}_0 , we observe the variation in the magnitude as vaccination rate for unmasked individuals ψ_1 is changed. Moreover, the vaccination rate for masked individuals is assumed to be six times greater than unmasked individuals ($\psi_2 = 6\psi_1$).

As shown in Figure 3.5, \mathcal{R}_0 decreases rapidly with increasing ψ_1 , dropping below the epidemic threshold of $\mathcal{R}_0 = 1$ at approximately $\psi_1 \approx 1.1 \times 10^{-3}$. Beyond this point, the curve flattens, indicating constant behaviour with further increases in the vaccination rate. From a public health standpoint, these findings emphasize the value of targeted vaccination campaigns focused on less compliant groups, as moderate increases in adherence to health interventions may be sufficient to suppress transmission. Once the threshold $\mathcal{R}_0 = 1$ is crossed, resources may be better directed toward sustaining coverage levels or improving other health interventions, such as further improvements to the vaccine efficacy or promoting mask adherence.

To explore how behavioural shifts between groups impact disease transmission, we analyze the effect of migration rates ω_{12} and ω_{21} on the overall basic reproduction number \mathcal{R}_0 . As illustrated in Figure 3.7, increasing the rate at which individuals move from the masked group to the unmasked group (ω_{21}) leads to a significant

increase in \mathcal{R}_0 . In contrast, increases in ω_{12} , which represent movement from the unmasked to the masked group, are associated with reductions in \mathcal{R}_0 . The white dashed curve, corresponding to $\mathcal{R}_0 = 1$, distinguishes the boundary between having a disease outbreak. The asymmetry in the relationship between ω_{12} and ω_{21} highlights the importance of promoting adherence to protective behaviours such as masking. From a public health standpoint, these results highlight that encouraging transitions toward mask compliance and minimizing riskier behaviours can play a critical role in avoiding disease outbreaks.

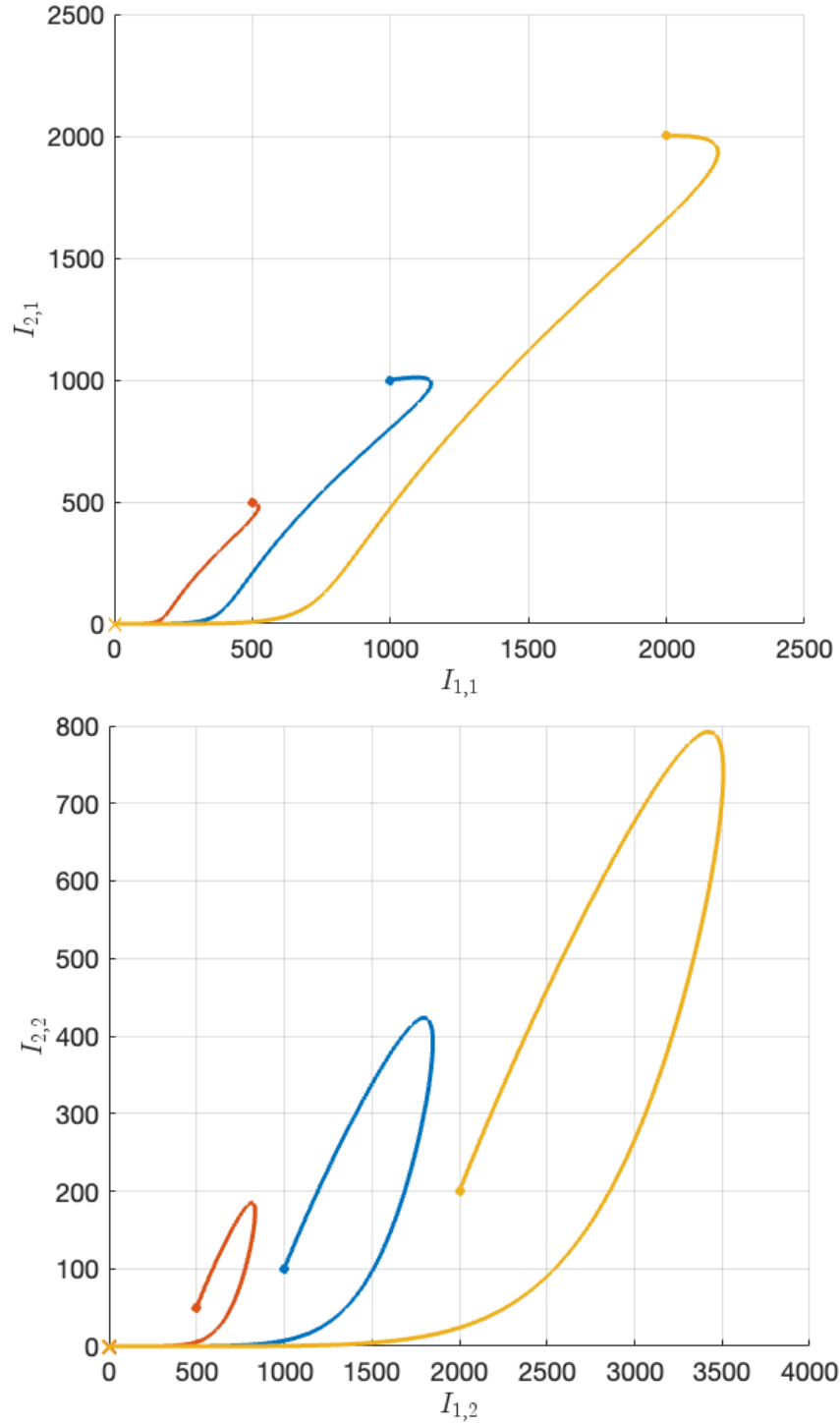


Figure 3.2: Phase portraits of symptomatic infections for strain 1 and strain 2 individuals in both unmasked (top) and masked groups (bottom). Each trajectory begins at an initial condition (solid dots) and converges to zero, indicating the local stability of the Disease-Free Equilibrium (DFE). The basic reproduction numbers for strain 1 and strain 2 are $\mathcal{R}_{0,1} = 0.724$ and $\mathcal{R}_{0,2} = 0.362$, respectively; thus, the overall basic reproduction number $\mathcal{R}_0 < 1$, ensuring disease elimination.

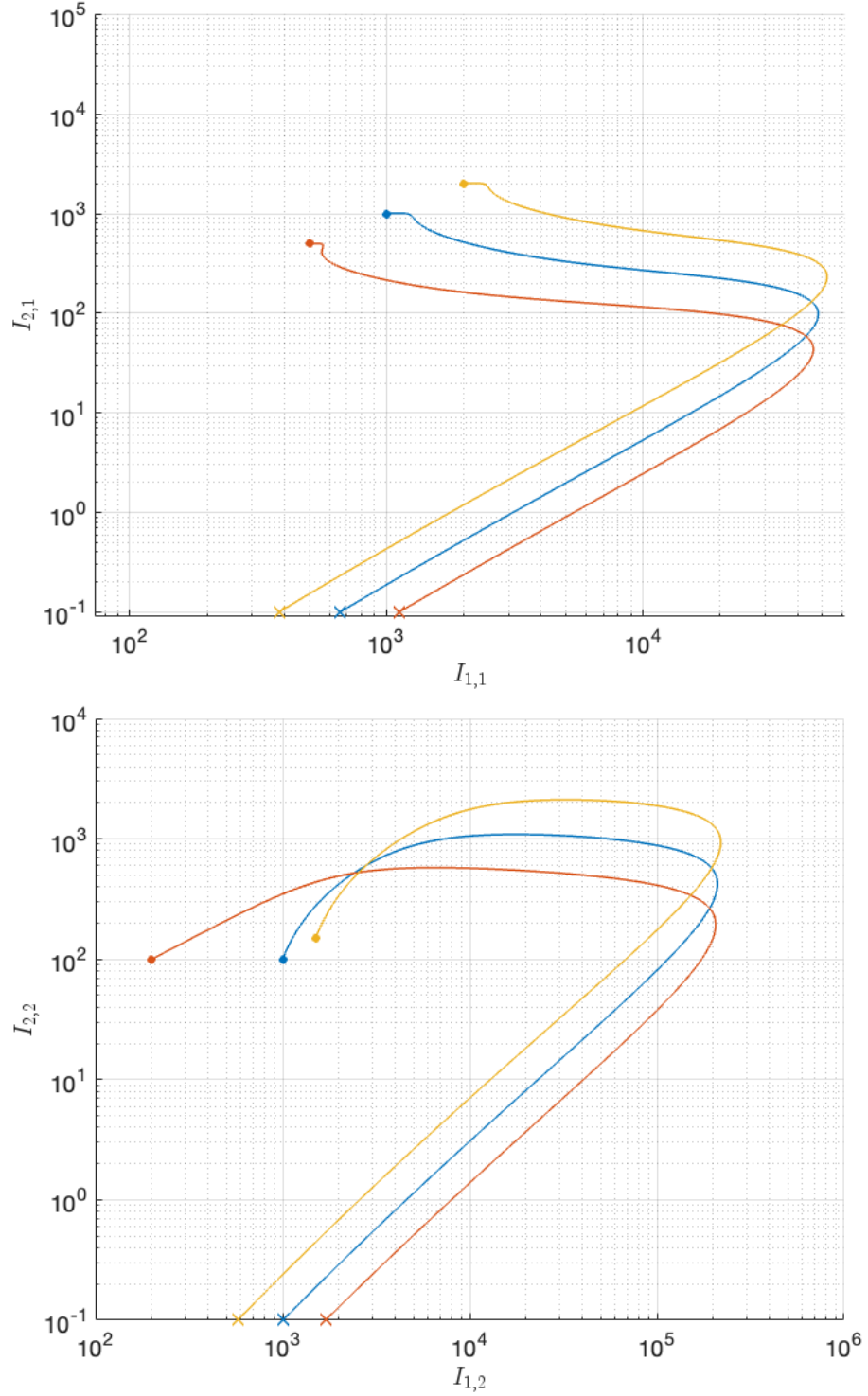


Figure 3.3: Log-scale phase portraits illustrating the solutions of symptomatic infections for strain 1 and strain 2 individuals in both unmasked (top) and masked groups (bottom). The strain-specific basic reproduction numbers are $\mathcal{R}_{0,1} = 1.429$ and $\mathcal{R}_{0,2} = 0.714$. Each trajectory corresponds to a different initial condition (solid dots). As shown, symptomatic infections of strain 2 diminish, while those of strain 1 converge to distinct non-zero values, signifying strain 1 dominance.

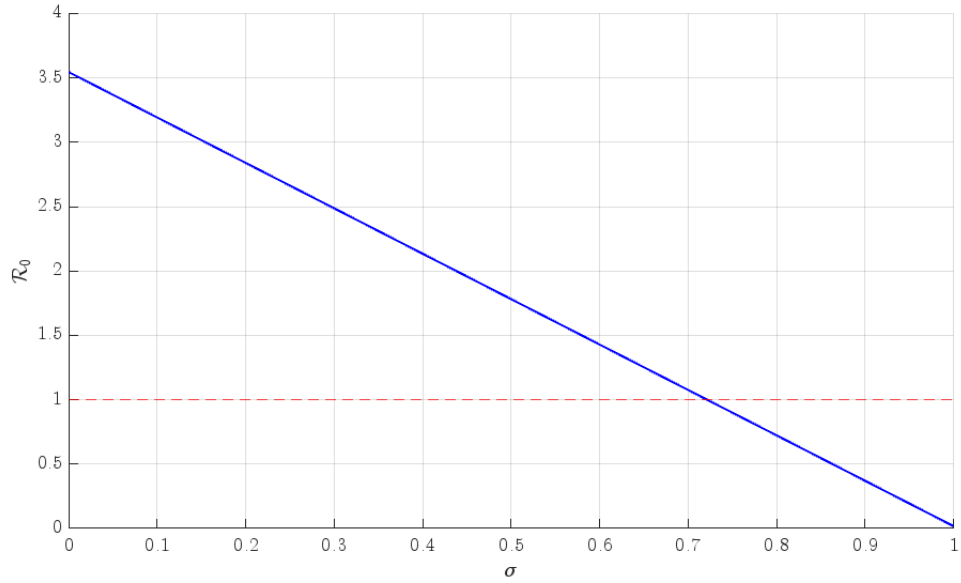


Figure 3.4: The influence of varying vaccine efficacy σ on the overall basic reproduction number \mathcal{R}_0 . The plot illustrates a linear decrease in \mathcal{R}_0 as vaccine efficacy improves and highlights the efficacy required to bring \mathcal{R}_0 below the threshold of 1 (dashed red line).

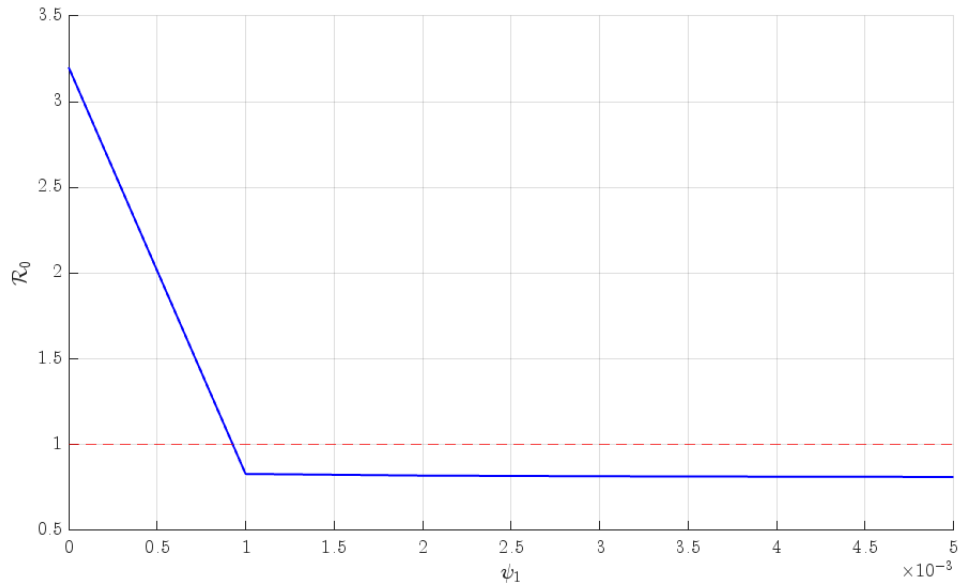


Figure 3.5: The overall basic reproduction number \mathcal{R}_0 as a function of the vaccination rate ψ_1 for unmasked individuals, with the vaccination rate for masked individuals fixed at six times ψ_1 , where $\psi_2 = 6\psi_1$. Vaccine efficacy is fixed at $\sigma = 0.75$. The dashed red line represents the epidemic threshold at $\mathcal{R}_0 = 1$, below which the disease spread is effectively controlled.

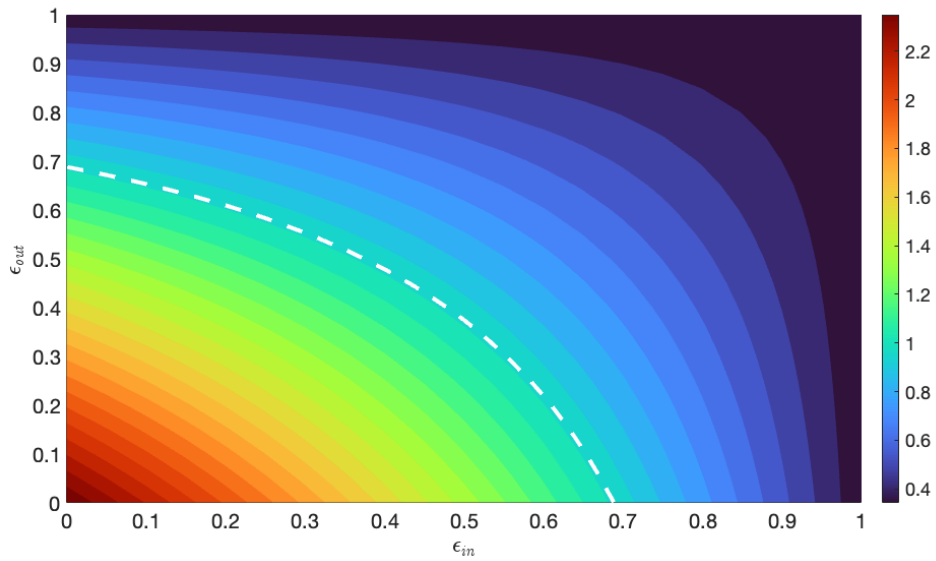


Figure 3.6: Contour plot showcasing variations of the overall basic reproduction number \mathcal{R}_0 as function of inward efficacy ϵ_{in} and outward efficacy ϵ_{out} of masks. Warmer colours (pale green to dark red) indicate higher values of \mathcal{R}_0 and cooler regions (pale blue to dark purple) signify lower values. The white dotted line represents the threshold value $\mathcal{R}_0 = 1$.

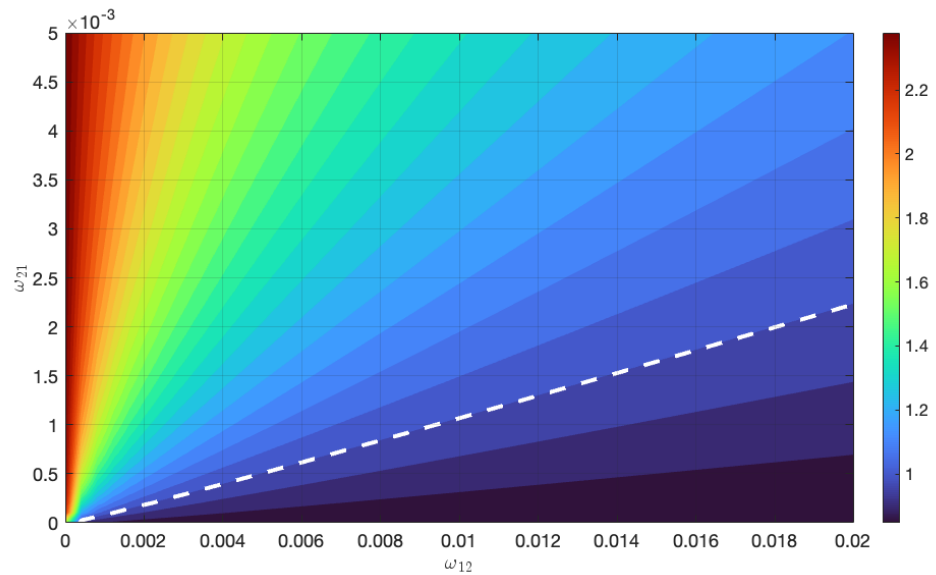


Figure 3.7: Contour plot of the overall basic reproduction number \mathcal{R}_0 illustrating its dependence on the migration rates ω_{12} (movement from the unmasked group to the masked group) and ω_{21} (movement from the masked group to the unmasked group). The dashed white line represents the critical threshold $\mathcal{R}_0 = 1$, below which the epidemic is controlled. Higher migration from the masked to the unmasked group (ω_{21}) notably increases the risk of disease spread.

Chapter 4

Conclusions and future work

The studies detailed in Chapter 2 and Chapter 3 present a rigorous approach to developing epidemic models that capture how a disease behaves with and without health interventions. The first model introduced in this thesis is a multi-strain SIARS model (2.1.3) that includes no health interventions. By extending model (2.1.3) to include masking and vaccinations as the health interventions of interest, model (3.1.3) was developed. Both models effectively integrate dynamics associated to asymptomatic infections in addition to symptomatic infections.

The first model studied in Chapter 2 explores three different classifications of steady states, namely: The disease-free equilibrium, strain-dominant equilibria and strain-coexistence equilibria. For each type of equilibrium, we have introduced existence and local stability conditions except for strain-coexistence equilibria, where a purely numerical analysis illustrated neutrally stable behaviour of solutions to model (2.1.3).

As a result of the stability analyses for model (2.1.3), it provided critical insights into conditions required for the diminishing of all strains of a given disease and in the scenario of competition between strains, under which considerations can a single strain dominate or multiple strains can coexist in the absence of health interventions.

The second model investigated in Chapter 3, being an extension to the model discussed in Chapter 2, includes masks and vaccines. The inclusion of vaccinated-susceptible subpopulations and the separation of unmasked and masked individuals into distinct population groups allowed the exploration of the impact of non-pharmaceutical and pharmaceutical interventions in reducing the probability of new infections being created when coming in contact with symptomatic or asymptomatic infections. As a result, we were able to distinguish the necessary intervention levels that ensure the control of a given disease outbreak.

Despite the contributions from models (2.1.3) and (3.1.3) for modelling infectious diseases, certain limitations were identified and offer promising avenues for future research.

- **Further equilibria evaluations:** For the case of model (2.1.3), the global stability of each type of equilibrium remains an open problem; thus, future works include the formulation of valid Lyapunov functions. On the other hand, for model (3.1.3), further studies can be done to find all other possible equilibria in addition to the DFE, which can be followed by the local and global stability analyses for each equilibrium classification.
- **Parameter estimation from real data:** The numerical analyses conducted in Chapter 2 and Chapter 3 use approximations for parameters rather than values formed from real-world data. Future work that estimates parameter values from the latest data could significantly enhance predictive accuracy of models (2.1.3) and (3.1.3), which may reflect more realistic outcomes.
- **Group-specific parameter relationships:** Inspired by studies from Childs et al. [8] and Pan et al. [28], future work should explore nonlinearities between strain-specific and/or group-specific parameters as opposed to using purely

linear reduction factors, which could reflect more precise insights from model predictions.

- **Multi-patch dynamics:** The current formulation of model (3.1.3) includes recruitment into the population within a single localized patch/region and does not account for migration between distinct geographical patches. If model (3.1.3) is extended to incorporate such mobility dynamics, it captures more comprehensive disease spread patterns. As a result, regional control measures can be designed and enforced.
- **Consideration of underlying health conditions:** The models introduced in this thesis could be adapted to study the interaction between infectious and non-infectious diseases, which a person can be infected with at once (e.g., Diabetes and COVID-19). This could aid in identifying which categories of populations are at a higher risk and prioritizing resources.

In conclusion, the models presented in this thesis provide a good foundation for understanding infectious disease transmission under various conditions. However, there is considerable potential for refinement and extension. By incorporating the suggestions mentioned in this chapter for future work, it could lead to further enhanced public health interventions and better informed policy decisions in the context of emerging infectious diseases.

Bibliography

- [1] Mira Baude and Alf Kimms, *Modelling pandemic behavior with a network-SIRD approach*, Central European Journal of Operations Research **32** (2024), 521–541.
- [2] Rosemary J. Boyton and Daniel M. Altmann, *The immunology of asymptomatic SARS-CoV-2 infection: what are the key questions?*, 12 2021, pp. 762–768.
- [3] Fred Brauer, *Compartmental models in epidemiology*, Lecture Notes in Mathematics **1945** (2008), 19–79.
- [4] Andrew William Byrne, David McEvoy, Aine B Collins, Kevin Hunt, Miriam Casey, Ann Barber, Francis Butler, John Griffin, Elizabeth A Lane, Conor McAloon, Kirsty OBrien, Patrick Wall, Kieran A Walsh, and Simon J More, *Inferred duration of infectious period of SARS-CoV-2: rapid scoping review and analysis of available evidence for asymptomatic and symptomatic COVID-19 cases*, BMJ Open **10** (2020), no. 8.
- [5] Harren J. Campos, Michelle N. Raza, Jayrold P. Arcede, Joey Genevieve T. Martinez, and Randy L. Caga-anan, *Vaccination and variants: A COVID-19 multi-strain model evolution for the Philippines*, Frontiers in Applied Mathematics and Statistics **9** (2023).
- [6] Centers for Disease Control and Prevention, *COVID-19 Timeline*, 2023.

- [7] Hiam Chemaitelly, Nico Nagelkerke, Houssein H. Ayoub, Peter Coyle, Patrick Tang, Hadi M. Yassine, Hebah A. Al-Khatib, Maria K. Smatti, Mohammad R. Hasan, Zaina Al-Kanaani, Einas Al-Kuwari, Andrew Jeremijenko, Anvar Hassan Kaleeckal, Ali Nizar Latif, Riyazuddin Mohammad Shaik, Hanan F. Abdul-Rahim, Gheyath K. Nasrallah, Mohamed Ghaith Al-Kuwari, Adeel A. Butt, Hamad Eid Al-Romaihi, Mohamed H. Al-Thani, Abdullatif Al-Khal, Roberto Bertollini, and Laith J. Abu-Raddad, *Duration of immune protection of SARS-CoV-2 natural infection against reinfection*, Journal of Travel Medicine **29** (2022).
- [8] Lauren Childs, David W Dick, Zhilan Feng, Jane M Heffernan, Jing Li, and Gergely Röst, *Modeling waning and boosting of COVID-19 in Canada with vaccination*, Epidemics **39** (2022), 100583.
- [9] Pyoeng Gyun Choe, Chang Kyung Kang, Hyeon Jeong Suh, Jongtak Jung, Kyoung Ho Song, Ji Hwan Bang, Eu Suk Kim, Hong Bin Kim, Sang Won Park, Nam Joong Kim, Wan Beom Park, and Myoung Don Oh, *Waning antibody responses in asymptomatic and symptomatic SARS-CoV-2 infection*, Emerging Infectious Diseases **27** (2021), 327–329.
- [10] Sebastián Contreras, H Andrés Villavicencio, David Medina-Ortiz, Juan Pablo Biron-Lattes, and Álvaro Olivera-Nappa, *A multi-group SEIRA model for the spread of COVID-19 among heterogeneous populations*, Chaos, Solitons & Fractals **136** (2020), 109925.
- [11] D Cucinotta and M Vanelli, *WHO Declares COVID-19 a Pandemic*, Acta Biomed **91** (2020), no. 1, 157–160.
- [12] Robert G.S. de Araújo, Daniel C.P. Jorge, Rejane C. Dorn, Gustavo Cruz-Pacheco, M. Lourdes M. Esteva, and Suani T.R. Pinho, *Applying a multi-strain dengue model to epidemics data*, Mathematical Biosciences **360** (2023).

- [13] Valeria De Giorgi, Kamille A. West, Amanda N. Henning, Leonard N. Chen, Michael R. Holbrook, Robin Gross, Janie Liang, Elena Postnikova, Joni Trenbeath, Sarah Pogue, Tania Scinto, Harvey J. Alter, and Cathy Conry Cantilena, *Naturally Acquired SARS-CoV-2 Immunity Persists for up to 11 Months following Infection*, *Journal of Infectious Diseases* **224** (2021), 1294–1304.
- [14] Adjodah Dhaval and Karthik A N D Chinazzi Matteo A N D Fraiberger Samuel P A N D Pentland Alex A N D Bates Samantha A N D Staller Kyle A N D Vespignani Alessandro A N D Bhatt Deepak L Dinakar, *Association between COVID-19 outcomes and mask mandates, adherence, and attitudes*, *PLOS ONE* **16** (2021), no. 6, 1–26.
- [15] Steffen E Eikenberry, Marina Mancuso, Enahoro Iboi, Tin Phan, Keenan Eikenberry, Yang Kuang, Eric Kostelich, and Abba B Gumel, *To mask or not to mask: Modeling the potential for face mask use by the general public to curtail the COVID-19 pandemic*, *Infectious Disease Modelling* **5** (2020), 293–308.
- [16] Shasha Gao, Mingwang Shen, Xueying Wang, Jin Wang, Maia Martcheva, and Libin Rong, *A multi-strain model with asymptomatic transmission: Application to COVID-19 in the US*, *Journal of Theoretical Biology* **565** (2023), 111468.
- [17] Yair Goldberg, Micha Mandel, Yinon M. Bar-On, Omri Bodenheimer, Laurence S. Freedman, Nachman Ash, Sharon Alroy-Preis, Amit Huppert, and Ron Milo, *Protection and Waning of Natural and Hybrid Immunity to SARS-CoV-2*, *New England Journal of Medicine* **386** (2022), 2201–2212.
- [18] Abba B Gumel, Enahoro A Iboi, Calistus N Ngonghala, and Gideon A Ngwa, *Toward Achieving a Vaccine-Derived Herd Immunity Threshold for COVID-19 in the U.S.*, *Frontiers in Public Health* **9** (2021).

- [19] Florian Huemer, Gabriel Rinnerthaler, Benedikt Jörg, Patrick Morre, Birgit Stegbuchner, Elisabeth Proksch, Stefanie Fleimisch, Hannes Oberkofler, Iris Kremser, Richard Greil, and Alexander Egle, *Results of a hospitalization policy of asymptomatic and pre-symptomatic COVID-19-positive long-term care facility residents in the province of Salzburg—a report from the AGMT COVID-19 Registry*, *GeroScience* **43** (2021), 1877–1897.
- [20] William Ogilvy Kermack, A G McKendrick, and Gilbert Thomas Walker, *A contribution to the mathematical theory of epidemics*, *Proceedings of the Royal Society of London. Series A, Containing Papers of a Mathematical and Physical Character* **115** (1927), no. 772, 700–721.
- [21] Teddy Lazebnik, *Computational applications of extended SIR models: A review focused on airborne pandemics*, 9 2023.
- [22] Mathilde Massard, Raluca Eftimie, Antoine Perasso, and Bruno Saussereau, *A multi-strain epidemic model for COVID-19 with infected and asymptomatic cases: Application to French data*, *Journal of Theoretical Biology* **545** (2022), 111117.
- [23] Mayu Nagata, Yuta Okada, and Hiroshi Nishiura, *Epidemiological impact of revoking mask-wearing recommendation on COVID-19 transmission in Tokyo, Japan*, *Infectious Disease Modelling* **9** (2024), 1289–1300.
- [24] Quynh C. Nguyen, Isha Yardi, Francia Ximena Marin Gutierrez, Heran Mane, and Xiaohe Yue, *Leveraging 13 million responses to the U.S. COVID-19 Trends and Impact Survey to examine vaccine hesitancy, vaccination, and mask wearing, January 2021-February 2022*, *BMC Public Health* **22** (2022).
- [25] Annett Nold, *Heterogeneity in disease-transmission modeling*, *Mathematical Biosciences* **52** (1980), no. 3, 227–240.

- [26] Stefania Ottaviano, Mattia Sensi, and Sara Sottile, *Global stability of multi-group SAIRS epidemic models*, *Mathematical Methods in the Applied Sciences* **46** (2023), no. 13, 14045–14071.
- [27] Olusegun Michael Otunuga, *Analysis of multi-strain infection of vaccinated and recovered population through epidemic model: Application to COVID-19*, *PLOS ONE* **17** (2022), no. 7, 1–45.
- [28] Jin Pan, Charbel Harb, Weinan Leng, and Linsey C. Marr, *Inward and outward effectiveness of cloth masks, a surgical mask, and a face shield*, *Aerosol Science and Technology* **55** (2021), 718–733.
- [29] Lawrence Perko, *Nonlinear Systems: Local Theory*, *Differential Equations and Dynamical Systems*, Springer New York, New York, NY, 2001, pp. 65–180.
- [30] Peter Rashkov and Bob W. Kooi, *Complexity of host-vector dynamics in a two-strain dengue model*, *Journal of Biological Dynamics* **15** (2021), 35–72.
- [31] Attiq ul Rehman, Ram Singh, and Jagdev Singh, *Mathematical analysis of multi-compartmental malaria transmission model with reinfection*, *Chaos, Solitons and Fractals* **163** (2022).
- [32] Duncan Scott and Paul A N D Naqvi Syed Bodurtha, *The protective performance of reusable cloth face masks, disposable procedure masks, KN95 masks and N95 respirators: Filtration and total inward leakage*, *PLOS ONE* **16** (2021), no. 10, 1–27.
- [33] Jianbin Tan, Yang Ge, Leonardo Martinez, Jimin Sun, Changwei Li, Adrianna Westbrook, Enfu Chen, Jinren Pan, Yang Li, Wei Cheng, Feng Ling, Zhiping Chen, Ye Shen, and Hui Huang, *Transmission roles of symptomatic and asymptomatic COVID-19 cases: A modelling study*, *Epidemiology and Infection* **150** (2022).

- [34] Lazebnik Teddy and Svetlana Bunimovich-Mendrazitsky, *Generic approach for mathematical model of multi-strain pandemics*, PLOS ONE **17** (2022), no. 4, 1–20.
- [35] P van den Driessche and James Watmough, *Reproduction numbers and sub-threshold endemic equilibria for compartmental models of disease transmission*, Mathematical Biosciences **180** (2002), no. 1-2, 29–48.
- [36] Jacqui Wise, *Global life expectancy to increase by almost five years by 2050, study predicts*, BMJ : British Medical Journal (Online) **385** (2024) (English).
- [37] World Health Organization, *COVID-19 Dashboard*, 2023.
- [38] Nana Wu, Keven Joyal-Desmarais, Paula A.B. Ribeiro, Ariany Marques Vieira, Jovana Stojanovic, Comfort Sanuade, Doro Yip, and Simon L. Bacon, *Long-term effectiveness of COVID-19 vaccines against infections, hospitalisations, and mortality in adults: findings from a rapid living systematic evidence synthesis and meta-analysis up to December, 2022*, The Lancet Respiratory Medicine **11** (2023), 439–452.
- [39] Lucas Zhou, Samuel K. Ayeh, Vignesh Chidambaram, and Petros C. Karakousis, *Modes of transmission of SARS-CoV-2 and evidence for preventive behavioral interventions*, BMC Infectious Diseases **21** (2021).

Vita

Candidate's full name: Ravindu Gimantha Upasena

Previous university attended: Monash University Malaysia - B.Eng (Honours)

Mechatronics Engineering - 2019

Publications: N/A

Conference Presentations: N/A